SF STATE

Kavli Institute for Theoretical Physics: Layering in Atmospheres, Oceans, and Plasmas
March 3, 2021

Dawn of the Zombie Vortex Instability

Dr. Joseph Barranco
Department of Physics & Astronomy
San Francisco State University
with
Philip Marcus (U.C. Berkeley)

Grant support from NSF-AST, computational resources from NSF-XSEDE

SF STATE

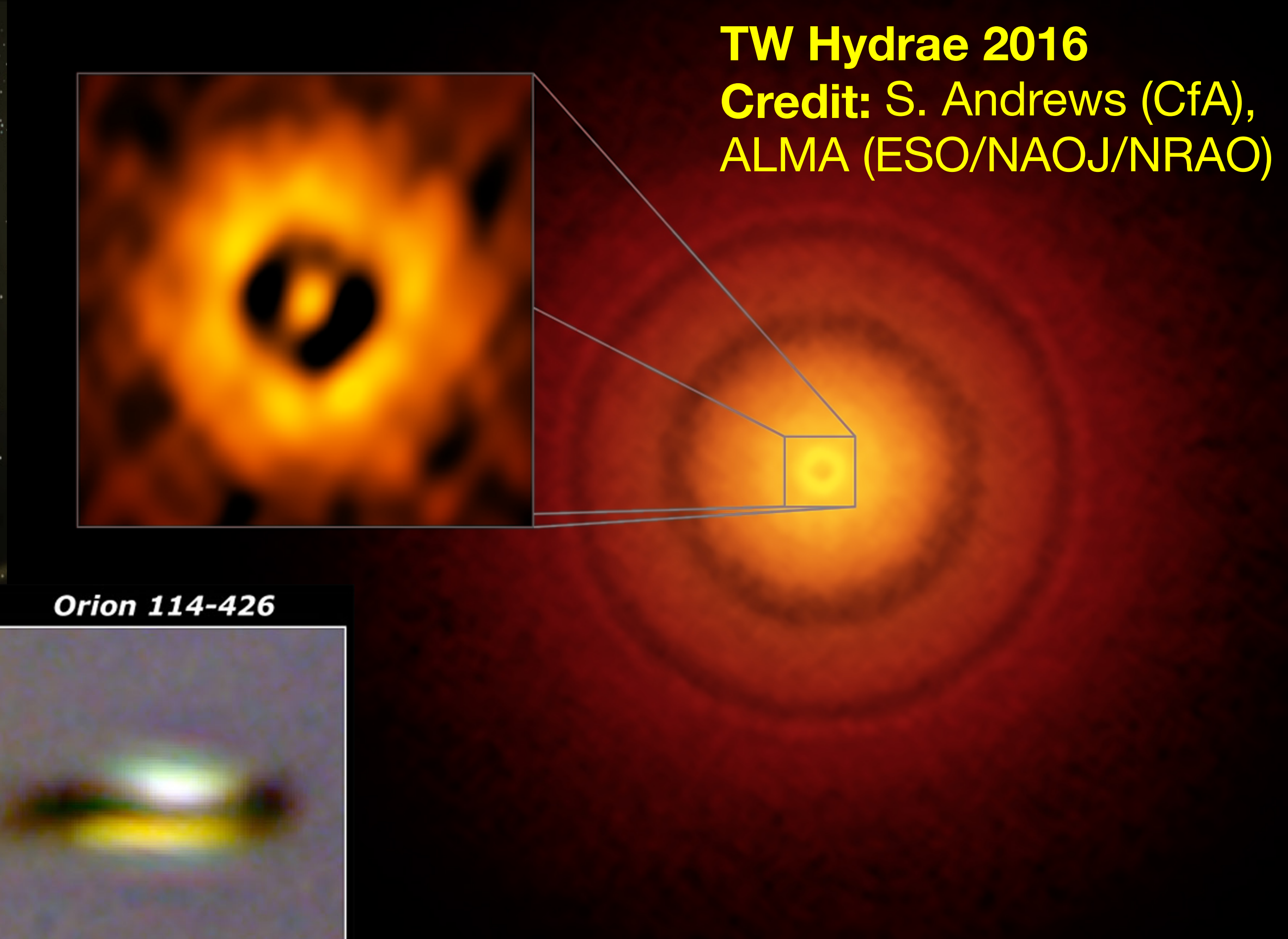

TW Hydrae 2016
Credit: S. Andrews (CfA), ALMA (ESO/NAOJ/NRAO)

Credit: Deborah Padgett, IPAC/Caltech, 1999

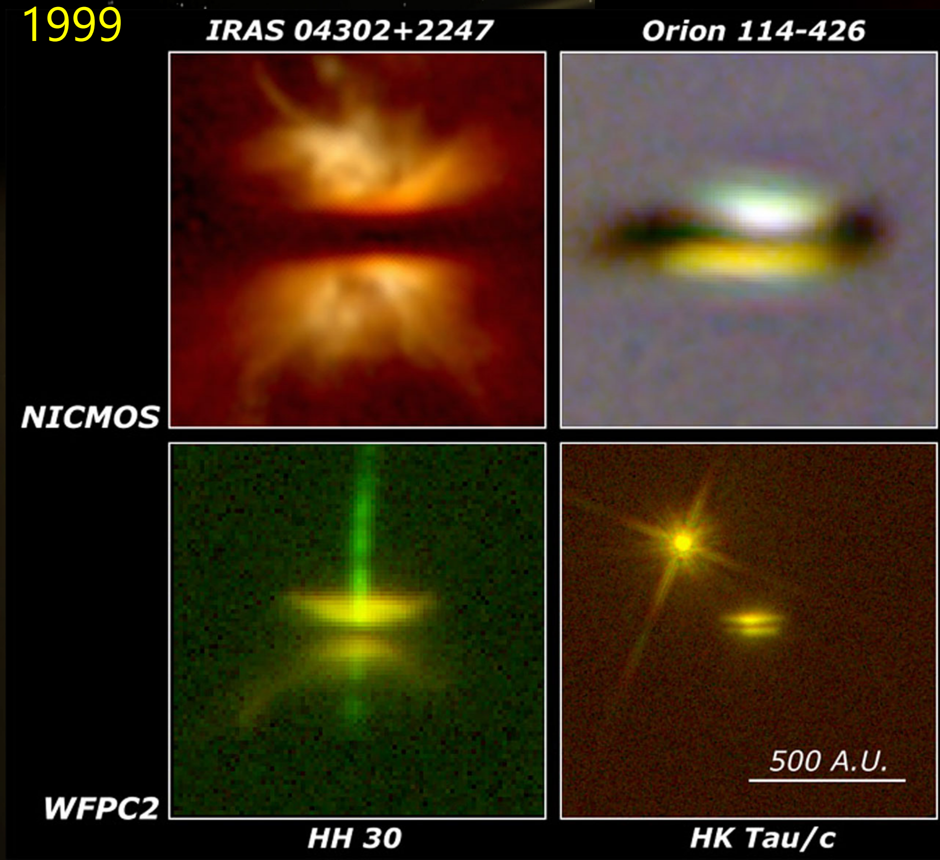

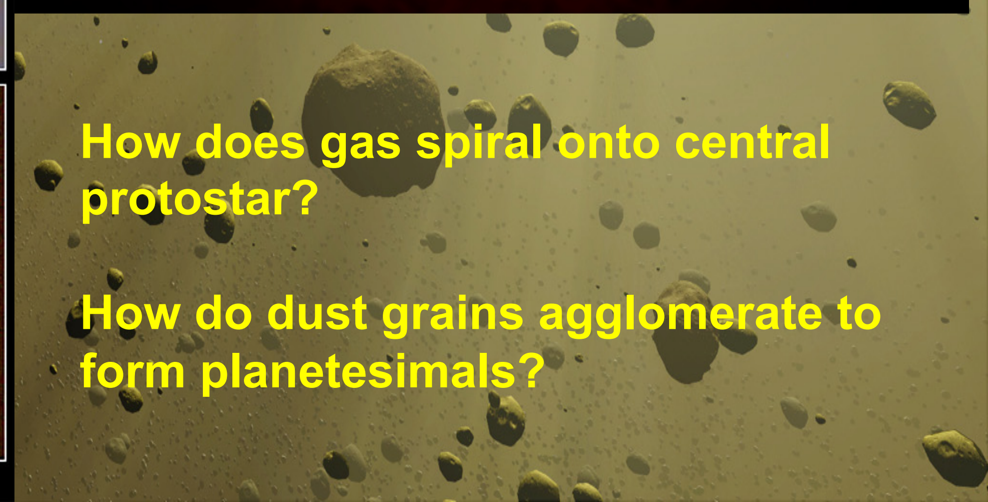

How does gas spiral onto central protostar?

How do dust grains agglomerate to form planetesimals?

Avenhaus et al.
DARTTS-S
collaboration
ESO
2018

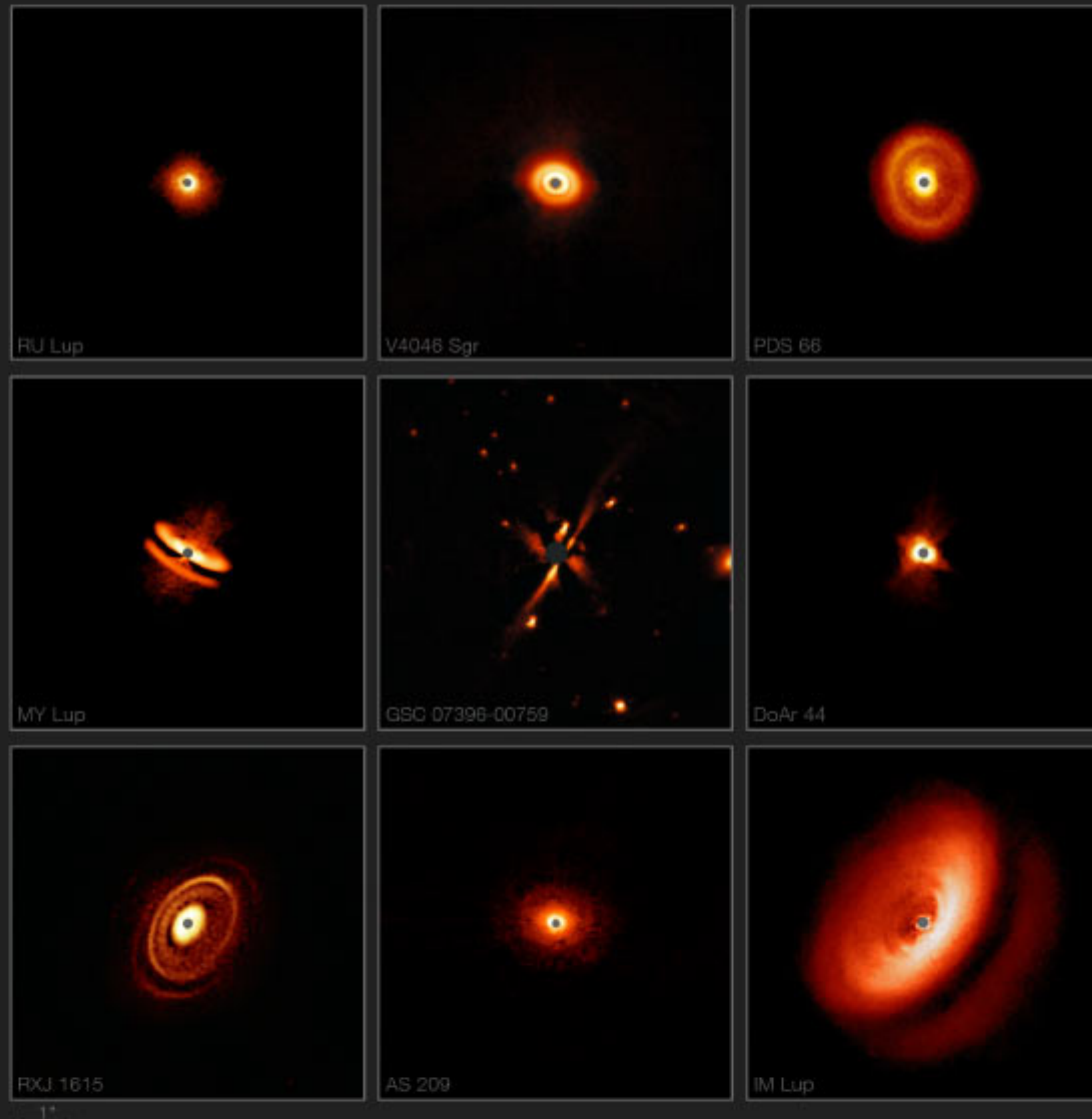

Protoplanetary Disks by the numbers…

- Size: few light-days across
- Aspect ratio $\delta \sim H/R \sim 0.03$
- Age: 5-20 million years
- 72% H_2, 26% He (by mass), 1% other gas, 1% dust
- $\rho \approx 10^{-6}$ kg/m^3 in midplane at 1 au
- $c_s \approx 1$ km/s, $v_{orb} = 30$ km/s at 1 au for 1 $M_\odot$
- $\lambda_{mfp} \approx 1$ cm for gas molecules; Re $\approx 10^{14}$
- dust particle size: μm to cm
- Average separation of dust particles: few cm
- In well-mixed state, in volume (100 m)^3, there is 1 kg of gas and few billion dust grains w/ size μm to cm

MHD "Dead" Zones

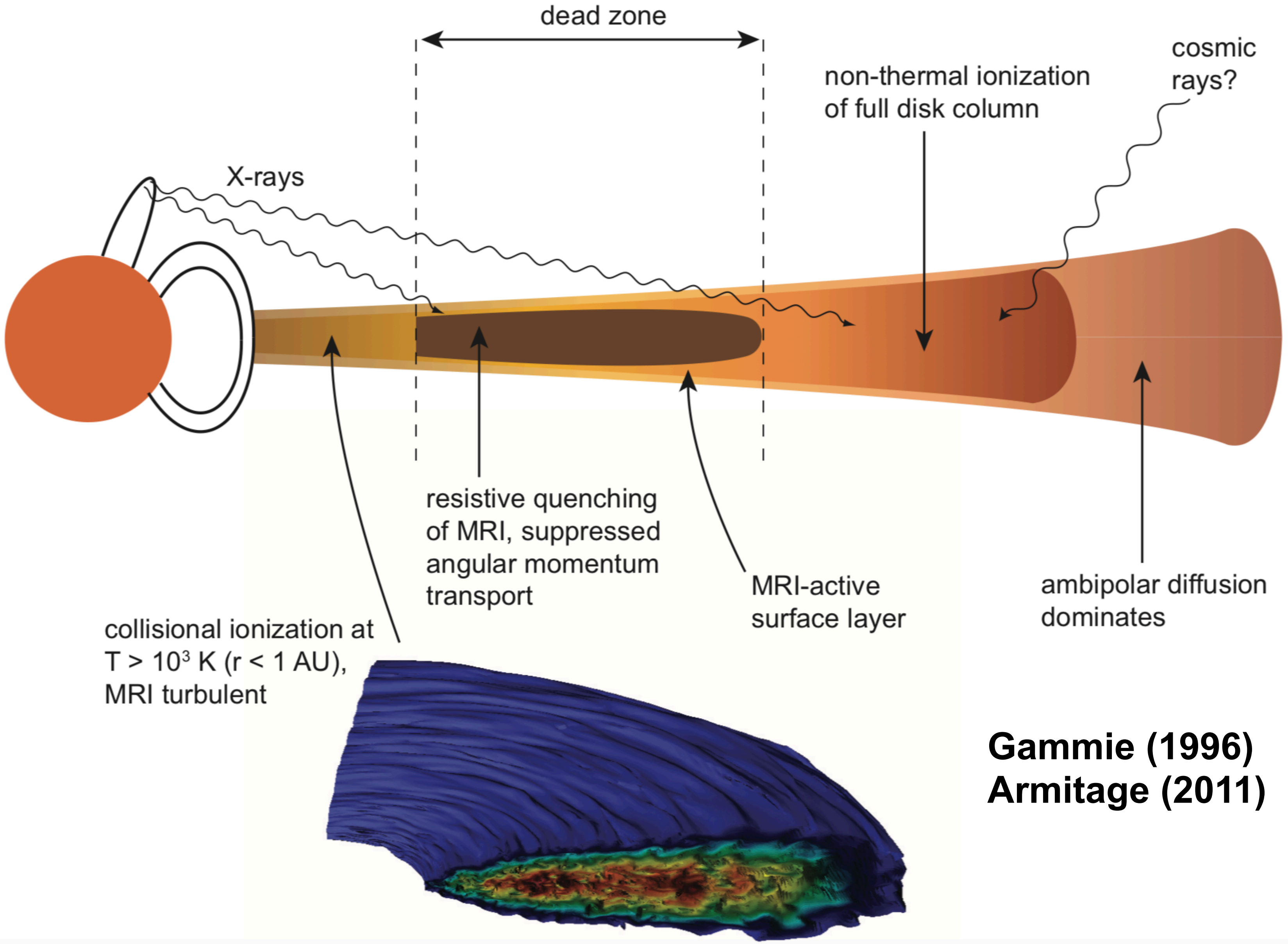

Gammie (1996)
Armitage (2011)

Jupiter's Great Red Spot

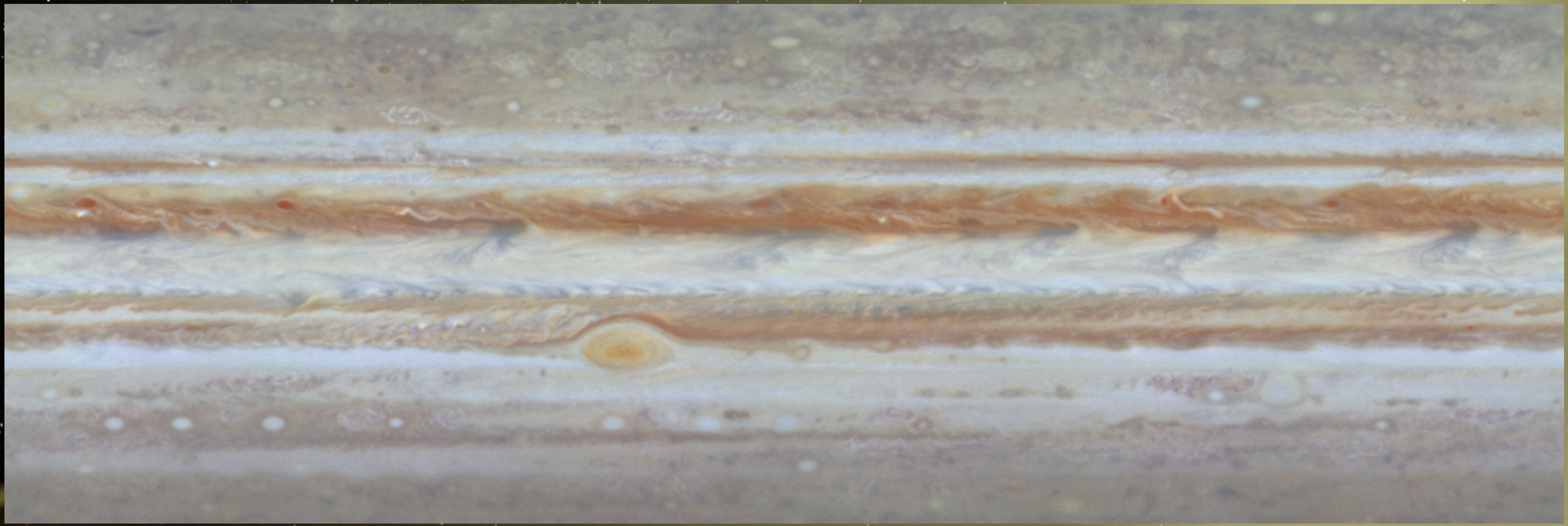

In nature, vortices thrive where there is:

- » Rapid rotation
- » Intense shear
- » Strong stratification

Jovian Vortices Versus Protoplanetary Disk Vortices

Timescale	GRS	PPD
$\tau_{vor} \equiv 4\pi/\omega$	8 days	≈ 1 orbit
$\tau_{orb} \equiv 2\pi/\Omega$	10 hours	≈ 1 orbit
$\tau_{BV} \equiv 2\pi/\omega_{BV}$	6 minutes	≈ 1 orbit
$Ro \equiv \tau_{orb}/\tau_{vor}$	0.18	≈ 1
$Fr \equiv \tau_{BV}/\tau_{vor}$	5×10^{-4}	≈ 1
$Ri \equiv 1/Fr^2$	4×10^{6}	≈ 1

Shearing Box Simulations

Box rotates with gas at radius r_0.

Keplerian differential rotation → Linear Shear

$V_y = -(3/2)\Omega_K x$

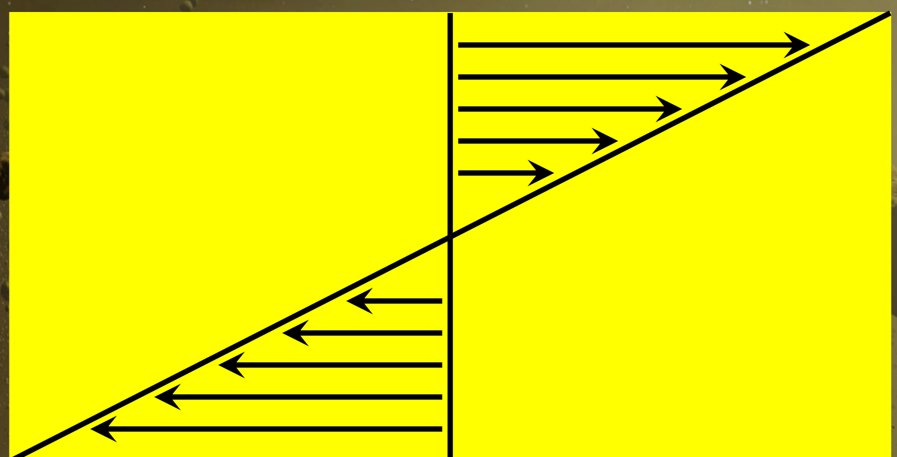

Hydrodynamic Equations

Consider a small box of gas in orbit around protostar. In this rotating reference frame, gas flow appears as a linear shear:

$$\bar{\boldsymbol{v}}(x) = \bar{v}_y(x)\hat{\boldsymbol{y}} = -\tfrac{3}{2}\Omega_0 x\hat{\boldsymbol{y}},$$
$$d(\ln\bar{p})/dz = -g_z(z)\bar{\rho}(z)/\bar{p}(z) = -(\Omega_0^2 z)/[\mathcal{R}\bar{T}(z)],$$

← Hydrostatic balance in vertical direction.

$$\bar{\theta}(z) = \bar{T}(z)[p_0/\bar{p}(z)]^{(\gamma-1)/\gamma},$$
$$[\bar{N}(z)]^2 = g_z(z)d(\ln\bar{\theta})/dz,$$

Stratification measured by potential temperature profile and the Brunt-Väisälä frequency.

Euler equations with anelastic approx. in rotating reference frame:

$$\partial\boldsymbol{v}/\partial t = -(\boldsymbol{v}\cdot\boldsymbol{\nabla})\boldsymbol{v} - 2\Omega_0\hat{\boldsymbol{z}}\times\boldsymbol{v} + 3\Omega_0^2\, x\hat{\boldsymbol{x}} - \boldsymbol{\nabla}\Pi + (\tilde{\theta}/\bar{\theta})g_z\hat{\boldsymbol{z}},$$
$$\partial\tilde{\theta}/\partial t = -(\boldsymbol{v}\cdot\boldsymbol{\nabla})\tilde{\theta} - v_z(\bar{\theta}\bar{N}^2/g_z) - \mathcal{L}_{rad}\tilde{\theta},$$
$$0 = \boldsymbol{\nabla}\cdot[\bar{\rho}(z)\boldsymbol{v}],$$

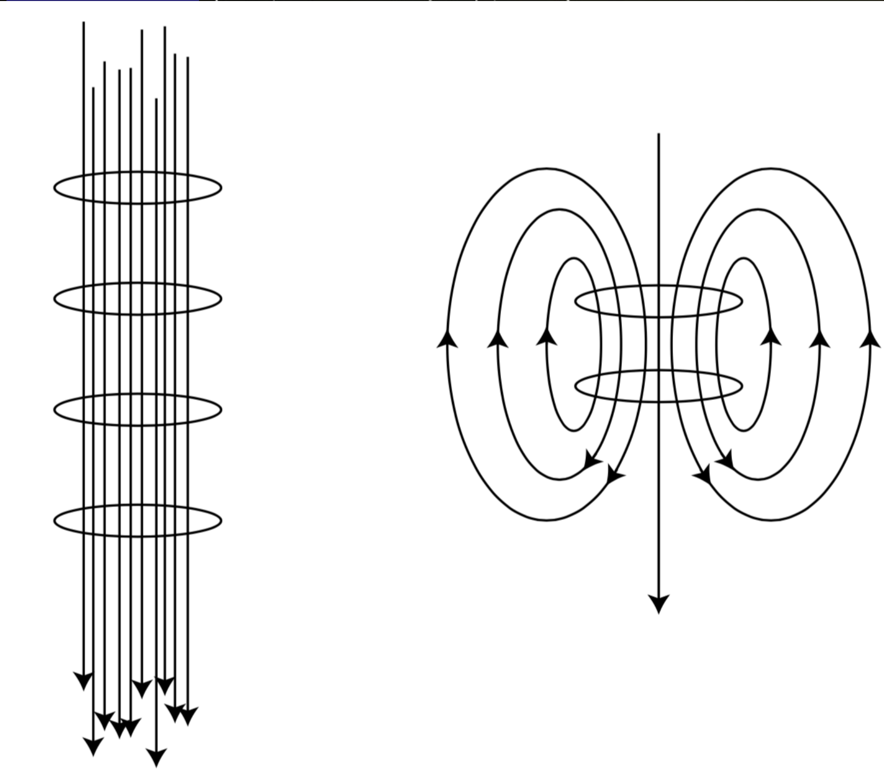

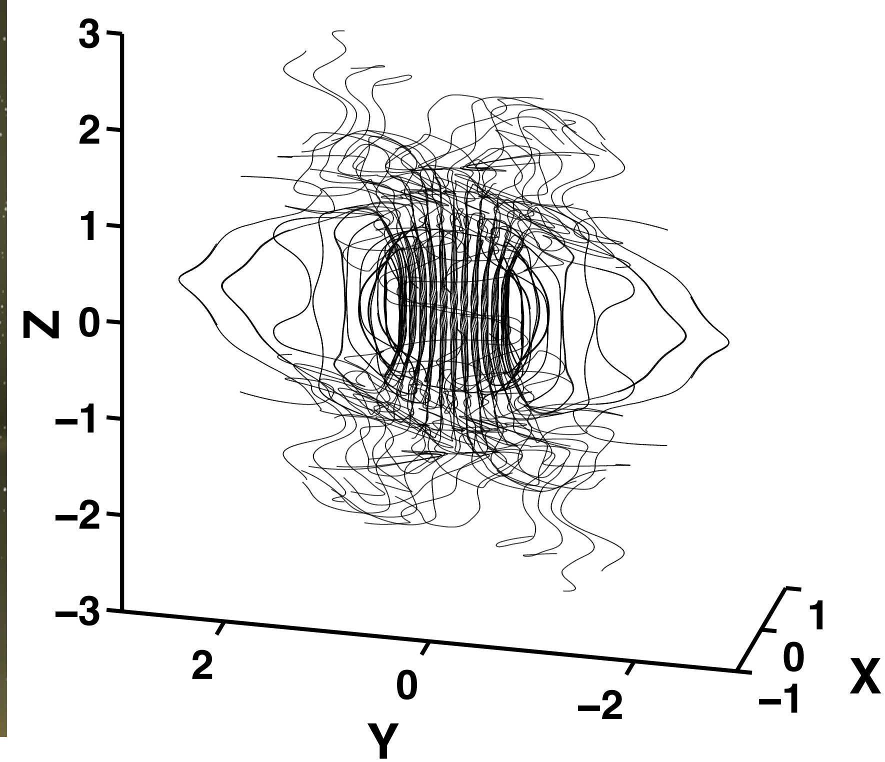

Because the vorticity is divergence free, vortex lines cannot end in the fluid but must form closed loops or go off to infinity! (Like magnetic field lines.)

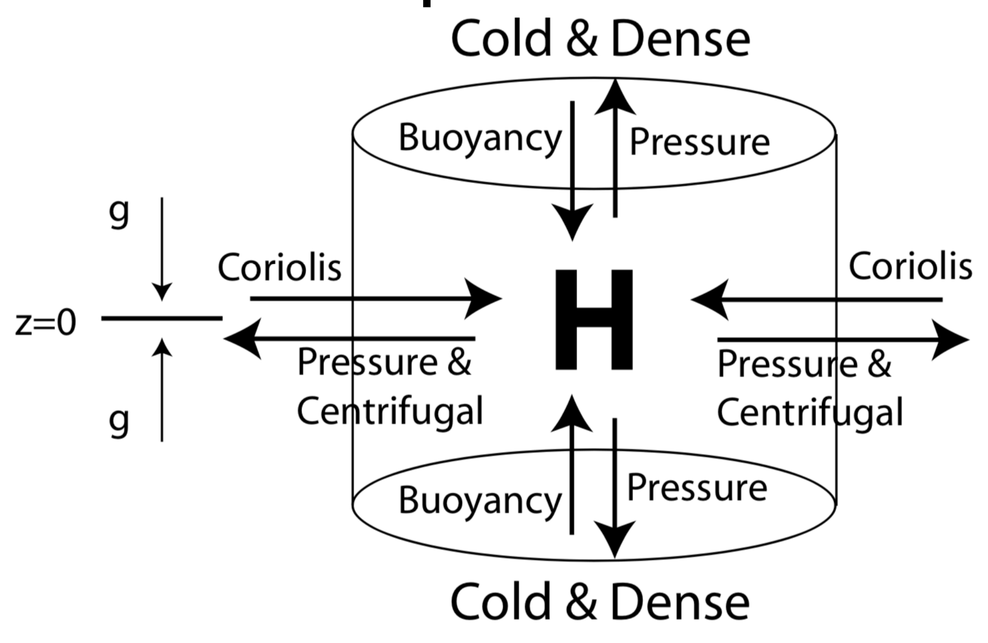

Short, hurricane-like vortex

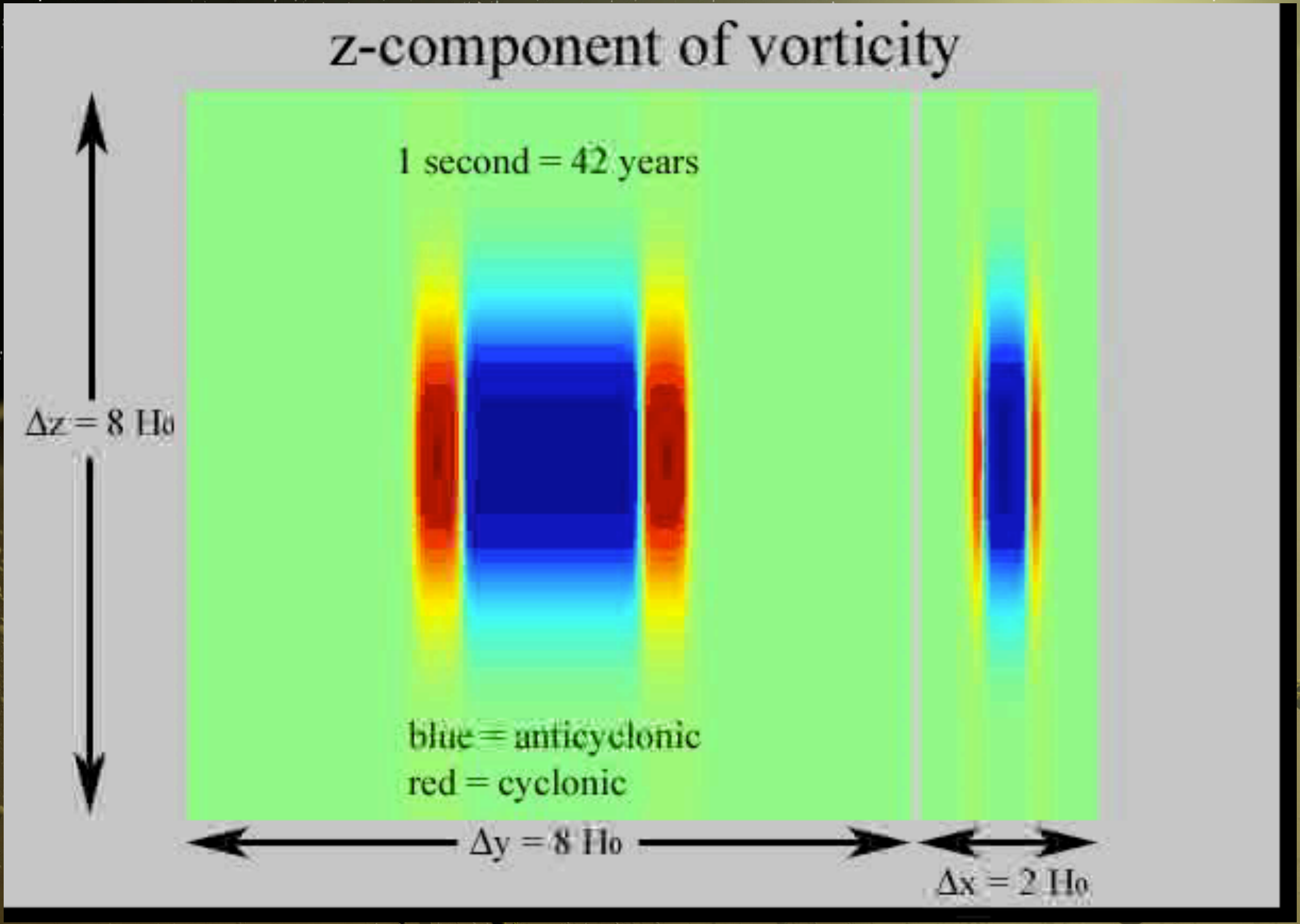

Barranco & Marcus (2005, 2006)

Short, hurricane-like vortex

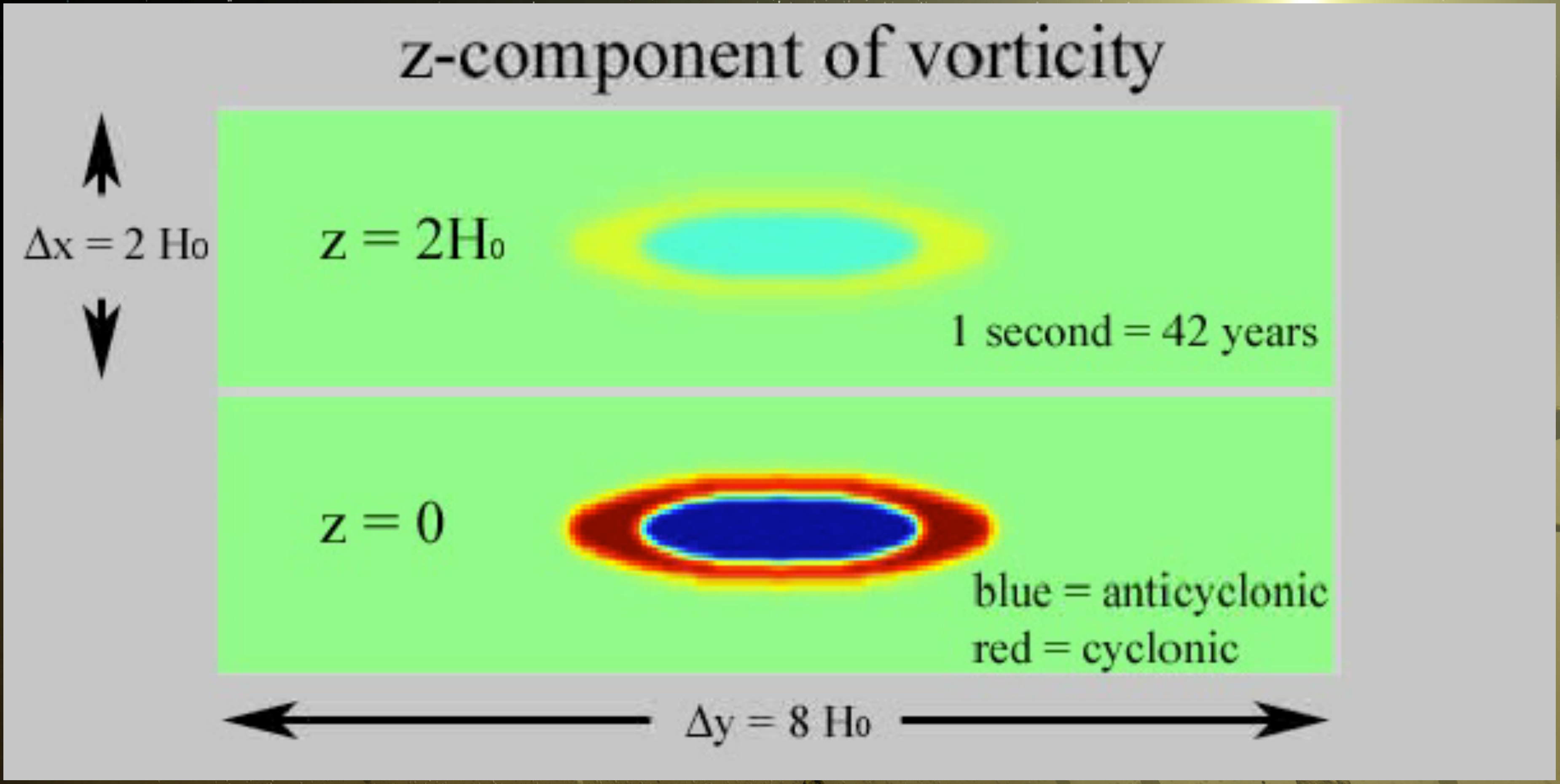

Barranco & Marcus (2005, 2006)

Dawn of the Zombie Vortex Instability

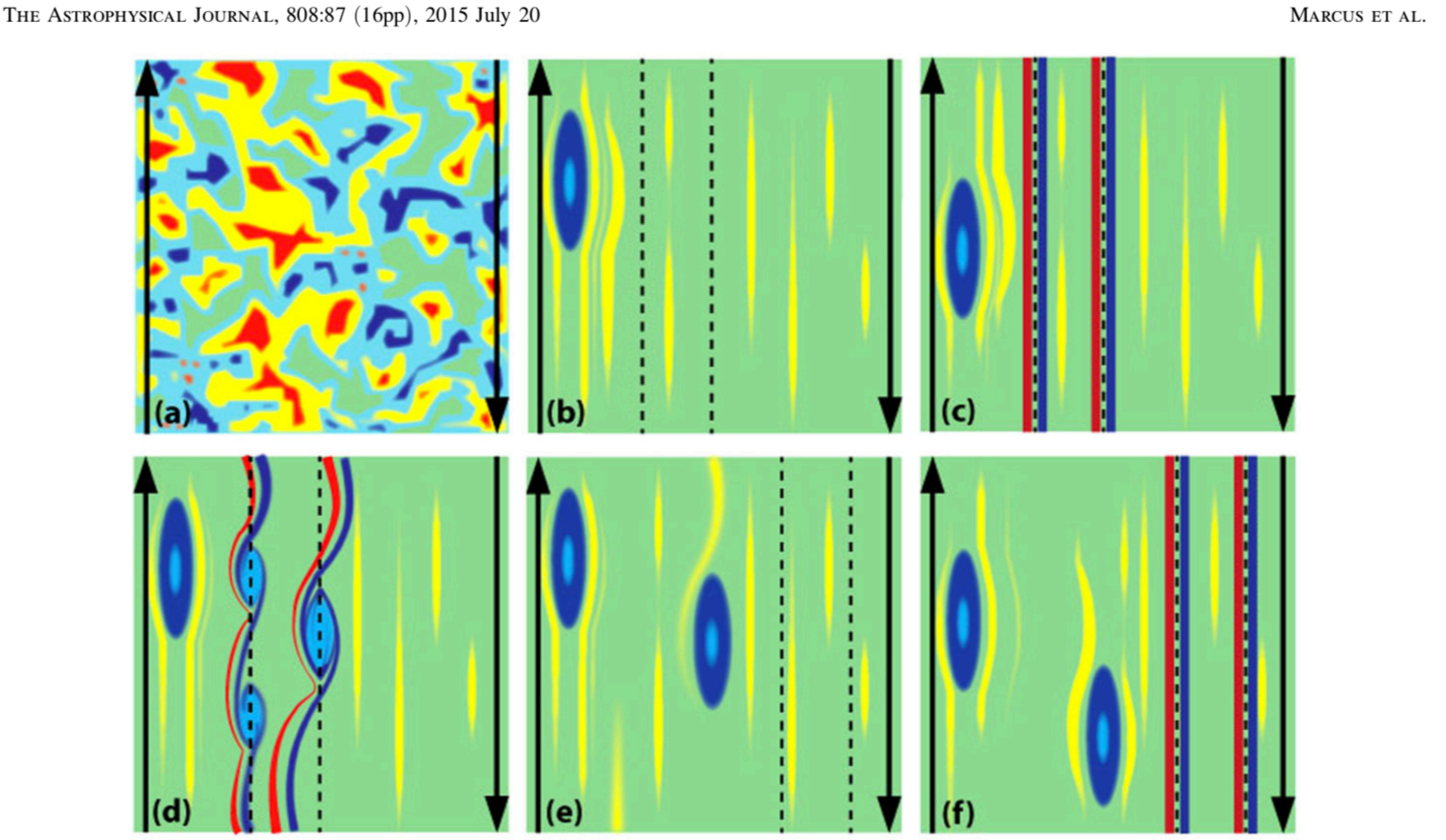

Marcus et al. 2013, 2015, 2016)

Baroclinic Critical Layers

$$\delta(m) \equiv \frac{N}{|\sigma|}\frac{1}{k_y} = \frac{N}{|\sigma|}\frac{L_y/2\pi}{m} \equiv \frac{\Delta}{m}$$

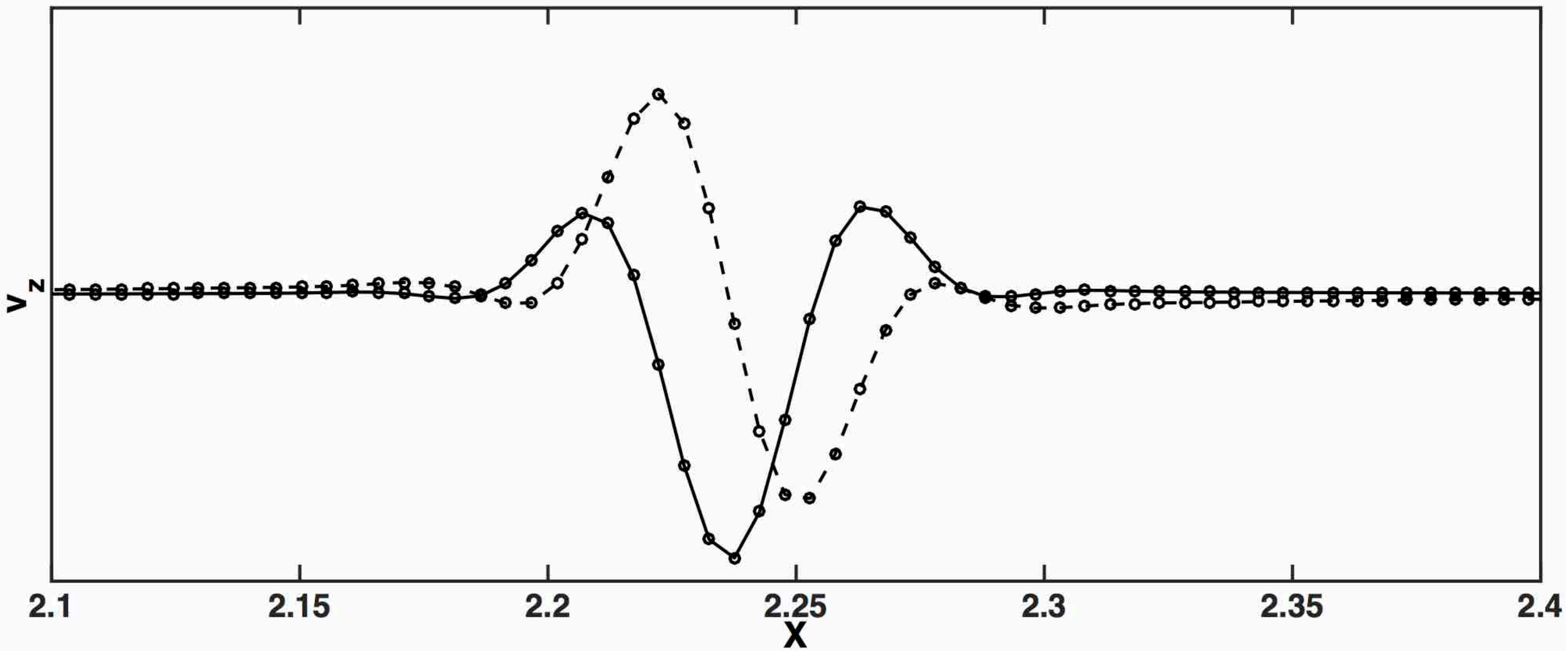

$$\frac{\partial \tilde{\omega}_z}{\partial t} + (v \cdot \nabla)\tilde{\omega}_z = (\tilde{\boldsymbol{\omega}}_\perp \cdot \nabla_\perp) v_z + \left(\tilde{\omega}_z + \frac{1}{2}\Omega_0\right)\frac{\partial v_z}{\partial z}$$

See Wang & Balmforth (2020): "Nonlinear Dynamics of Forced Baroclinic Layers"

Nonlinear trigger: Vorticity on small scale

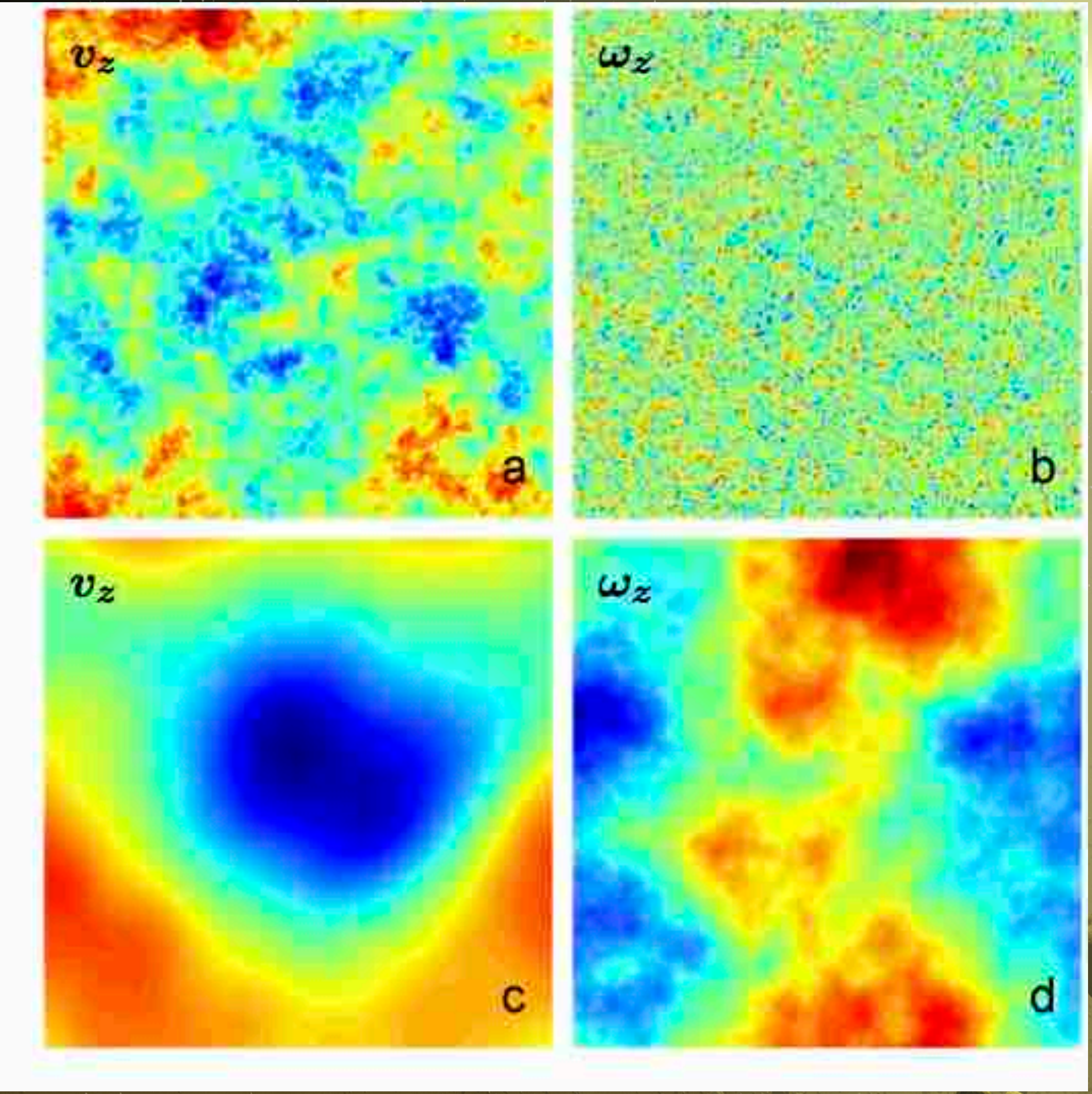

Why was instability missed for 30 years?

- Much of the early work on PPD dynamics ignored stratification. There was the belief that if a rotating flow is stable, a stratified rotating flow is even more stable (FALSE!)
- Need high resolution to resolve the very thin baroclinic critical layers.
- Instability is nonlinear and requires a broad spectrum of initial perturbations.
- Nonlinear evolution takes thousands of orbital periods; very few early calculations were ever evolved that long.

Dawn of the Zombie Vortex Instability

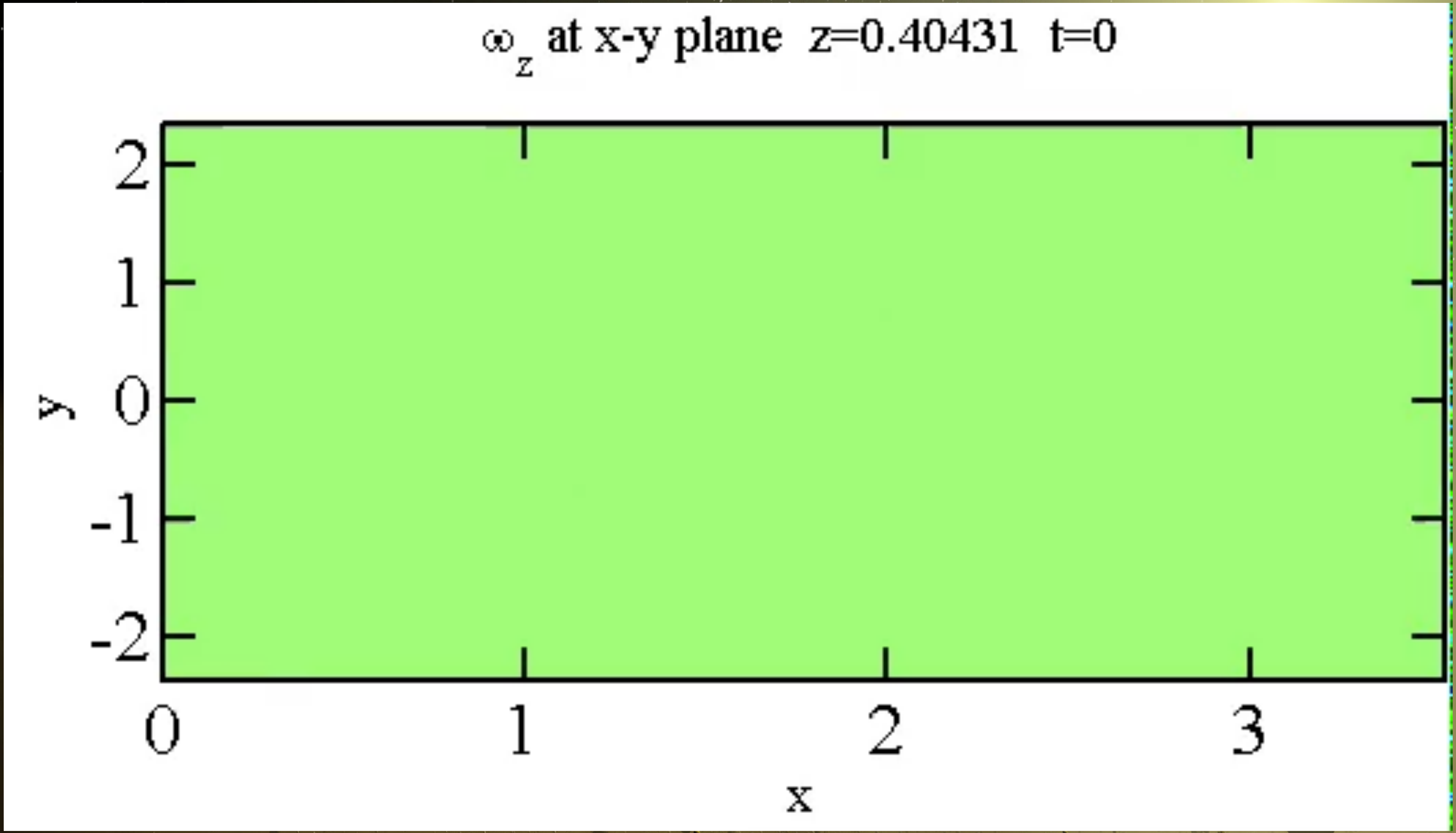

Marcus et al. (2013)

Dawn of the Zombie Vortex Instability

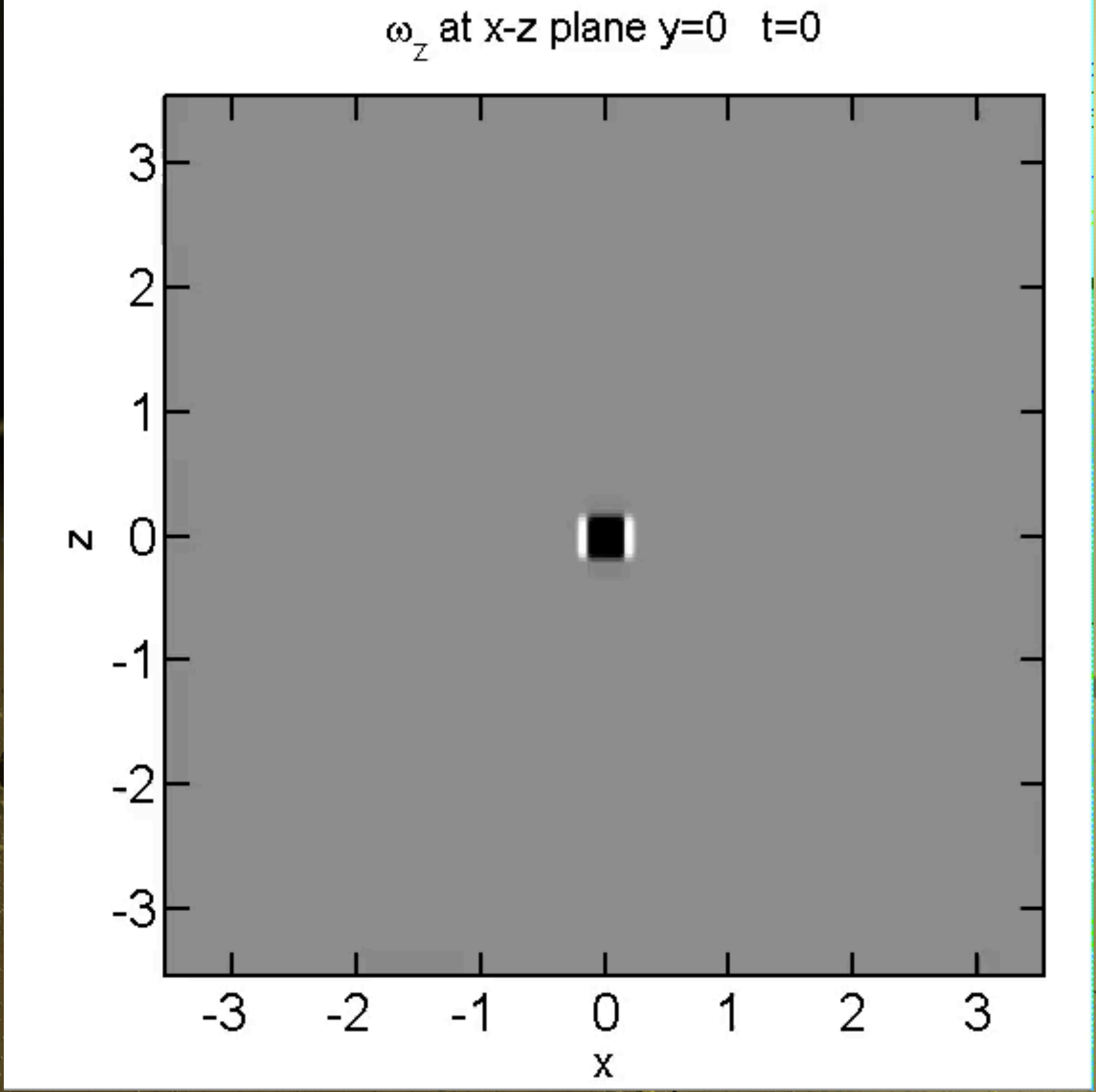

Marcus et al. (2013)

ZVI with non-uniform stratification

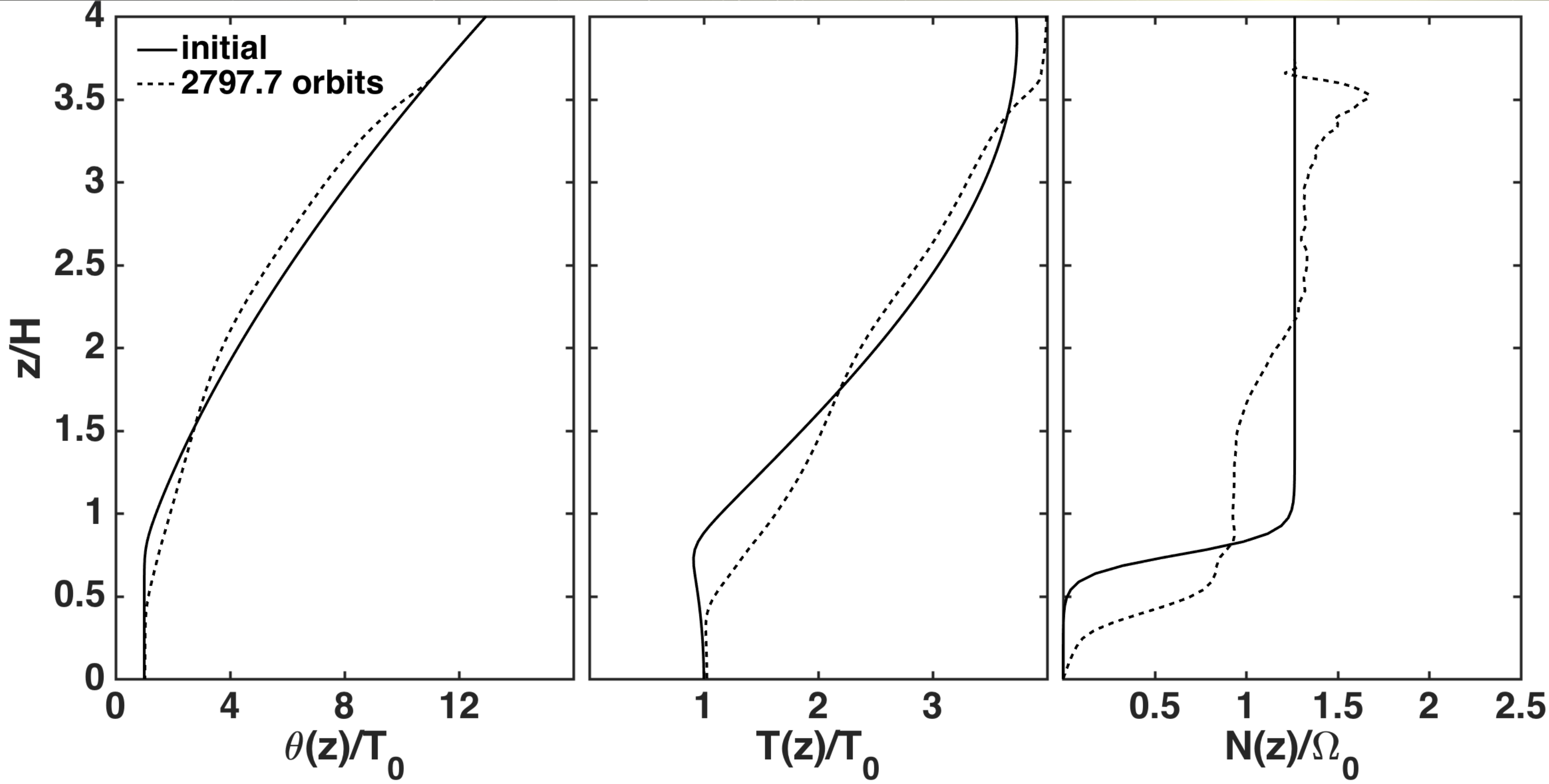

Barranco et al. (2018)
See also: Marcus et al. 2015, 2016)

ZVI with non-uniform stratification

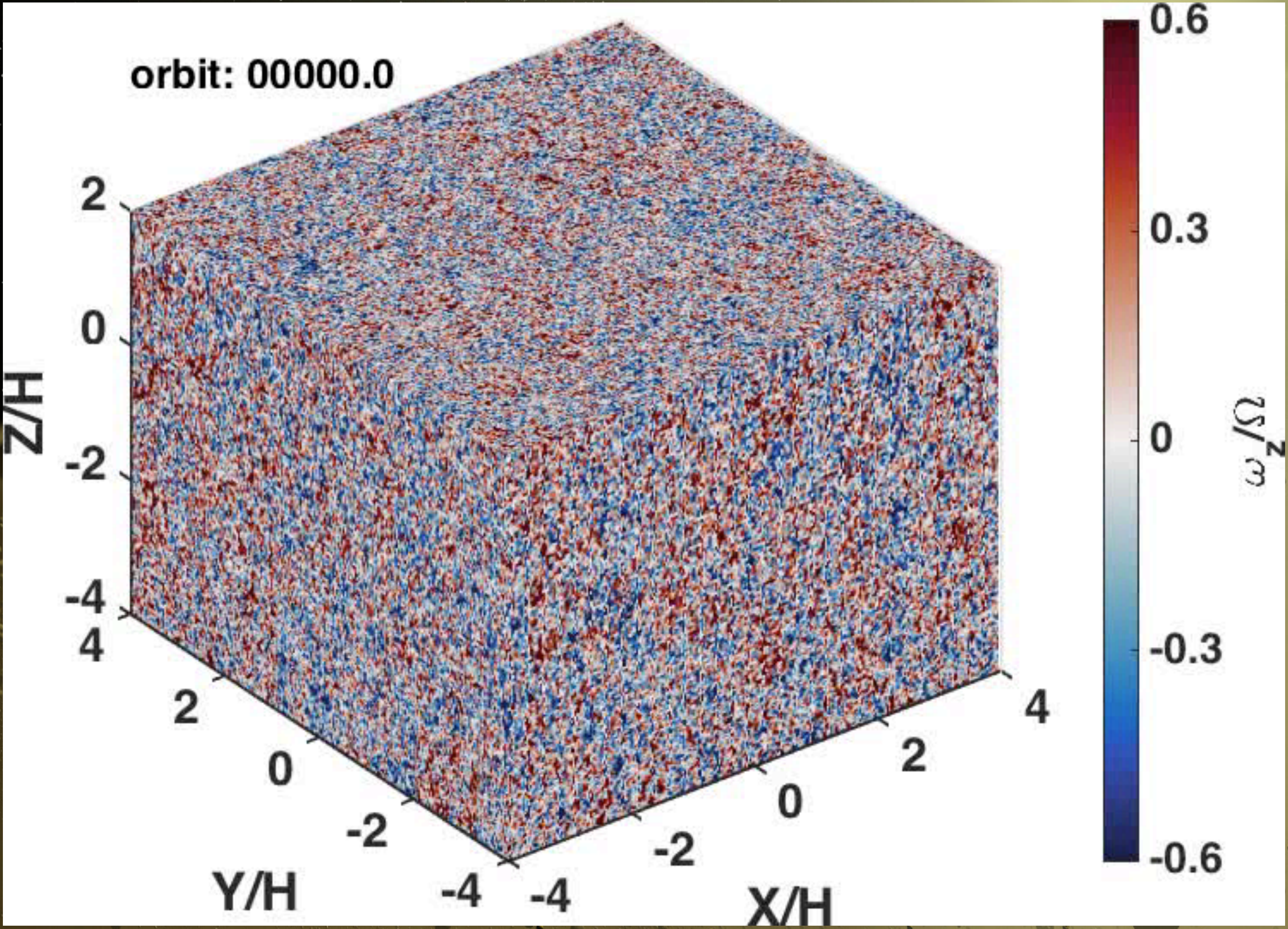

Barranco et al. (2018)
See also: Marcus et al. 2015, 2016)

SF STATE

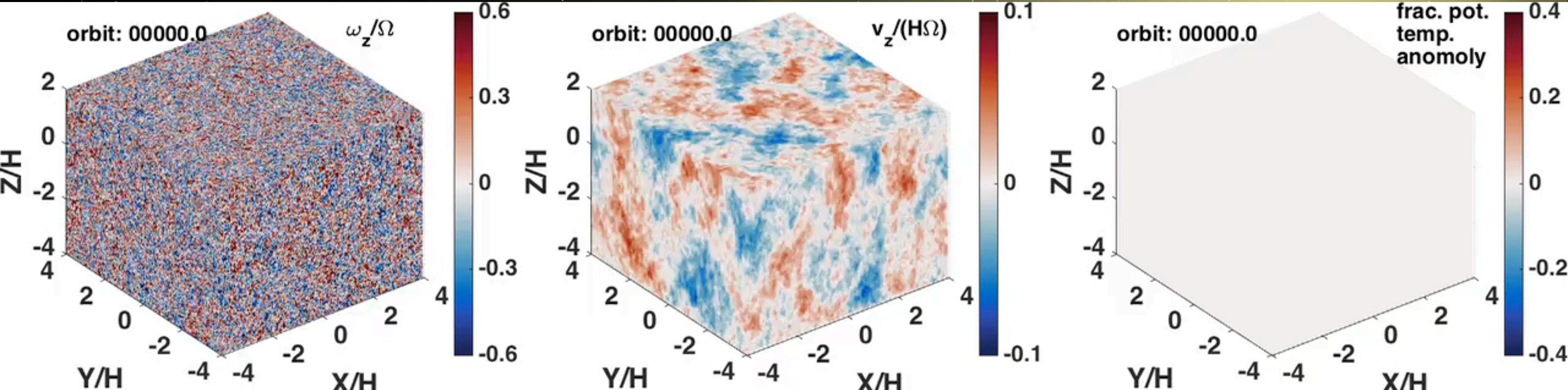
orbit: 00000.0
ω_z/Ω
0.6
0.3
0
-0.3
-0.6
Z/H
Y/H
X/H
orbit: 00000.0
$v_z/(H\Omega)$
0.1
0
-0.1
Z/H
Y/H
X/H
orbit: 00000.0
frac. pot.
temp.
anomoly
0.4
0.2
0
-0.2
-0.4
Z/H
Y/H
X/H

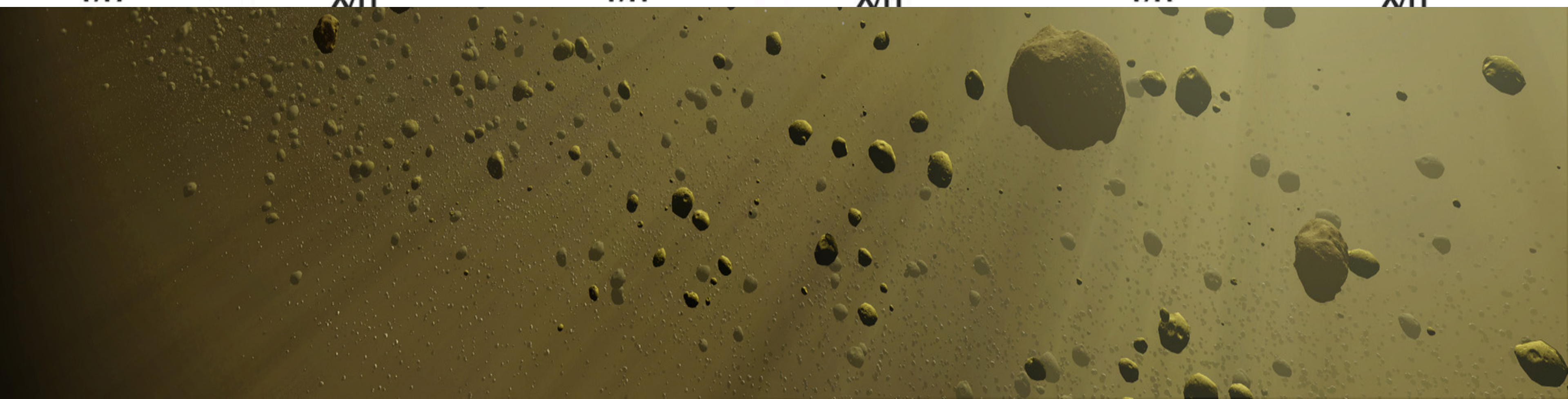

ZVI with non-uniform stratification

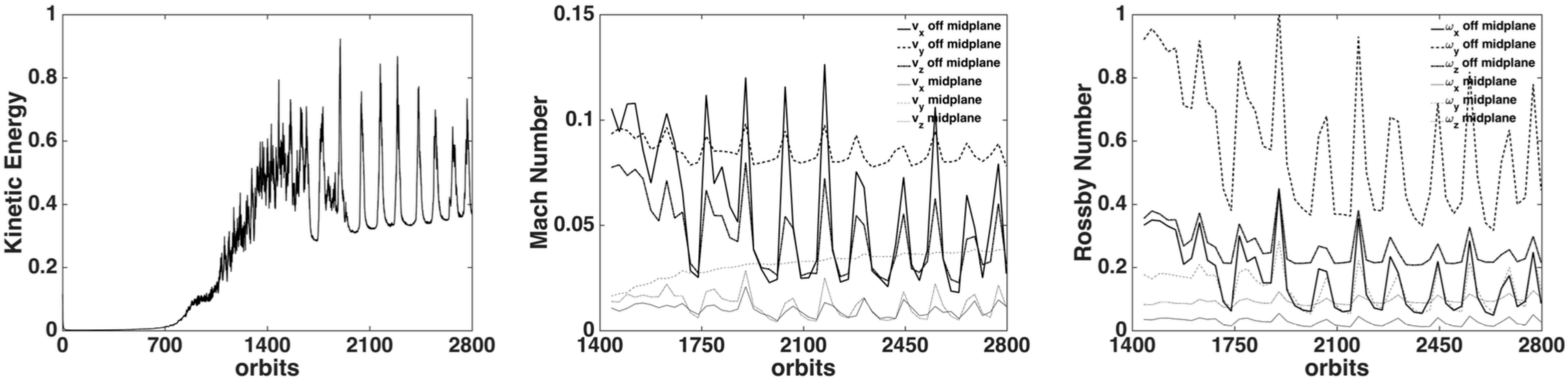

Turbulent bursts with period of 125 orbits!

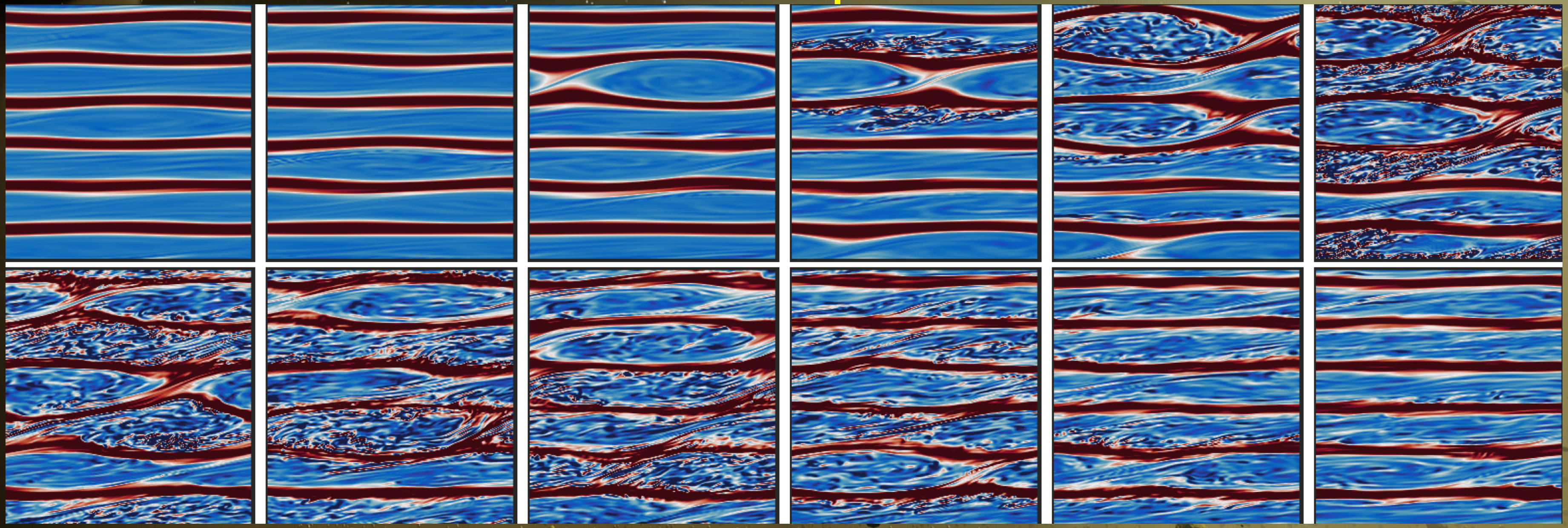

Barranco et al. (2018), See also: Marcus et al. 2015, 2016)

ZVI with non-uniform stratification

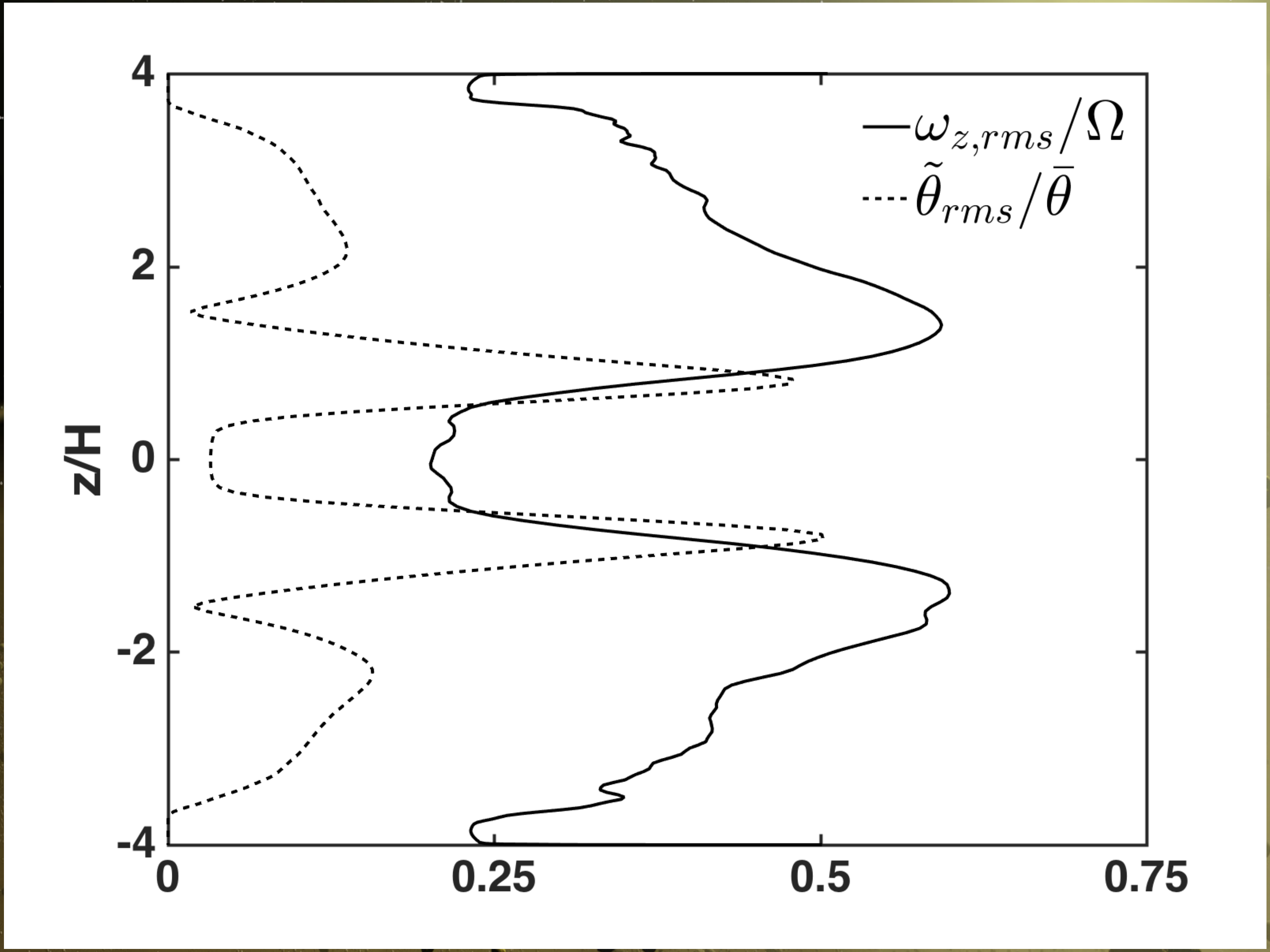

Barranco et al. (2018)
See also: Marcus et al. 2015, 2016)

ZVI with non-uniform stratification

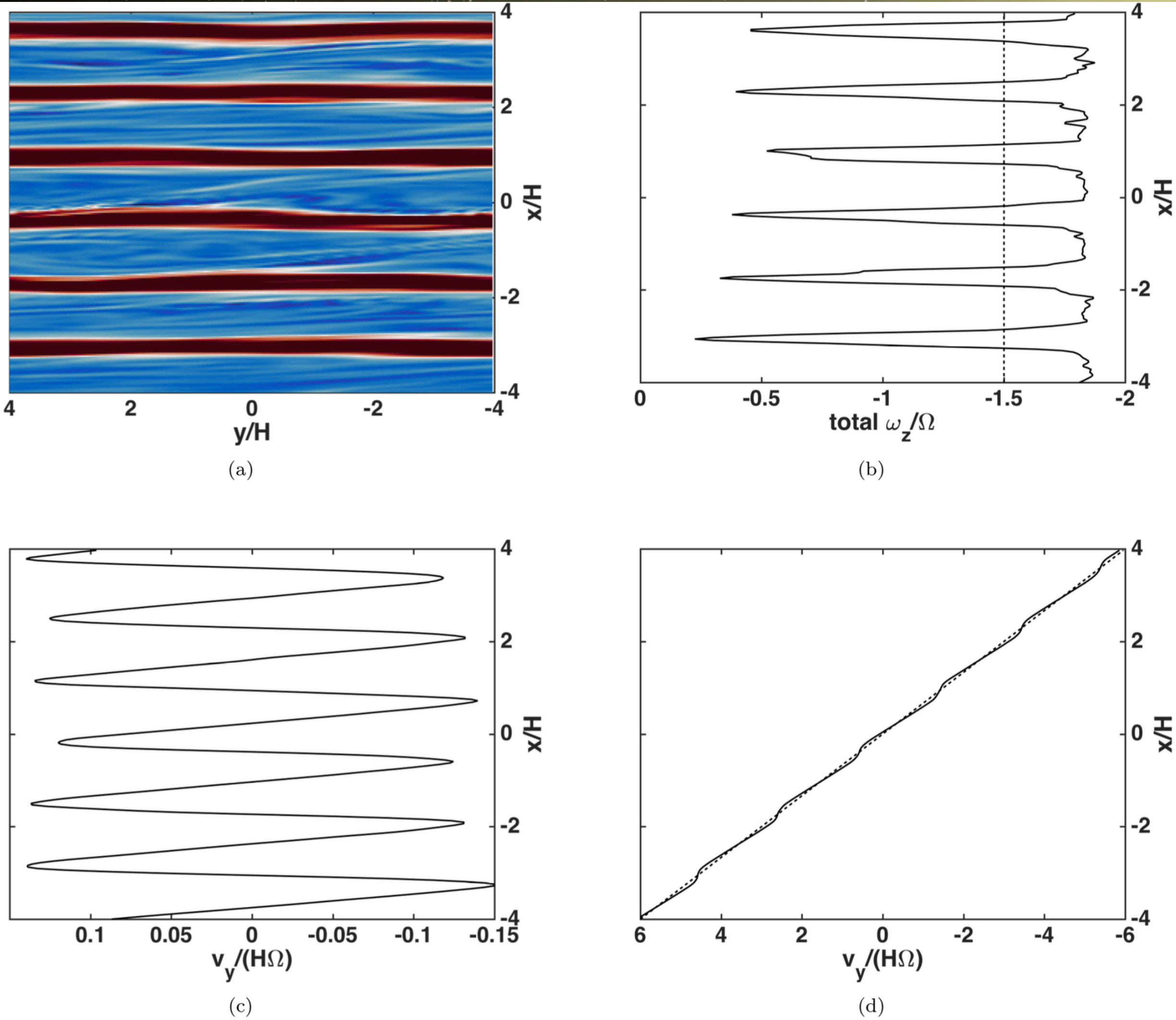

Figure 7. **Zonal flow in profile Run_Brunt_Step.** (a) Vertical component of relative vorticity in a horizontal plane at height $z = 2H_0$ after $\approx$ 2800 orbits. Colormap is the same as in Figure 3. (b) Azimuthally averaged vertical component of total vorticity in rotating frame. The total vorticity here is the relative vorticity plus the vorticity of the Keplerian shear, $\omega_{Kep} = -(3/2)\Omega_0$, indicated by the vertical dashed line. (c) Corresponding azimuthally averaged relative azimuthal velocity $v_y - v_{Kep}$. (d) Corresponding azimuthally averaged azimuthal velocity, including background Keplerian shear flow. Note that the graph in panel (b) is exactly the first derivative of the graph in panel (d).

Understanding Cooling Times

$$dT'_g/dt = -(T'_g - T'_d)/t_g^{col},$$
$$dT'_d/dt = +(T'_g - T'_d)/t_d^{col} - T'_d/t_d^{rad},$$

Gas and dust exchange energy via collisions, dust radiates energy in the infrared

$$1/t_{||} \equiv 1/t_g^{col} + 1/t_d^{col} + 1/t_d^{rad},$$
$$t_{relax} = 2t_{||}\left[1 - \sqrt{1 - 4t_{||}^2/t_g^{col}t_d^{rad}}\right]^{-1}$$
$$\approx t_g^{col}(1 + t_d^{rad}/t_d^{col})$$
$$\approx t_g^{col} + t_{thin}.$$

Understanding Cooling Times

$$t_{rad} = \frac{c_v}{16\kappa\sigma T^3}\frac{1}{(1-\tau\cot^{-1}\tau)},$$

Optical depth $\tau = \rho\kappa\ell$
Gas density ρ
Opacity κ
Physical length ℓ

Spiegel (1957)

$$t_{thin} = c_v/(16\kappa\sigma T^3) \propto 1/\kappa \qquad \text{for } \tau \ll 1,$$
$$t_{thick} = 3c_v\rho^2\kappa\ell^2/(16\sigma T^3) \propto \kappa\ell^2 \qquad \text{for } \tau \gg 1.$$

$\rho\kappa = n_d \pi a^2 Q_{IR}$
Emissivity $Q_{IR} \propto aT$

Infrared photon mean free path due to dust opacity:

$$\ell_{IR} = \frac{1}{\rho\kappa_d} = \frac{\rho_s}{\rho_d}\frac{(800\ \mu\mathrm{m}\cdot\mathrm{K})}{T} = 1600\ \mathrm{km}\left(\frac{T}{100\ \mathrm{K}}\right)^{-1}\left(\frac{\rho_d}{10^{-8}\ \mathrm{kg\ m^{-3}}}\right)^{-1},$$

Understanding Cooling Times

Rate of energy exchange between gas and dust via collisions:

$$\Lambda_{col} \approx \pi a^2 n_d n_g \bar{v}_g (2\mathcal{A}) k_B (T_g - T_d)$$

$$\approx 1.28 \times 10^{-5} \text{ W m}^{-3} \text{ K}^{-1} \left(\frac{a}{1\ \mu\text{m}}\right)^{-1} \left(\frac{\rho_d/\rho_g}{0.01}\right) \left(\frac{\rho_g}{10^{-6}\text{ kg m}^{-3}}\right)^2 \left(\frac{T_g}{100\text{ K}}\right)^{1/2} (T_g - T_d),$$

Response time ~ thermal energy content / energy exchange rate

$$t_g^{col} = \rho_g c_p / (\Lambda_{col}/|T_g - T_d|)$$

$$\approx 700\text{ s} \left(\frac{a}{1\ \mu\text{m}}\right) \left(\frac{\rho_d/\rho_g}{0.01}\right)^{-1} \left(\frac{\rho_g}{10^{-6}\text{ kg m}^{-3}}\right)^{-1} \left(\frac{T_g}{100\text{ K}}\right)^{-1/2},$$

$$t_d^{col} = \rho_d c_d / (\Lambda_{col}/|T_g - T_d|) = (\rho_d c_d / \rho_g c_p) t_g^{col}$$

$$\approx 0.7\text{ s} \left(\frac{a}{1\ \mu\text{m}}\right) \left(\frac{\rho_g}{10^{-6}\text{ kg m}^{-3}}\right)^{-1} \left(\frac{T_g}{100\text{ K}}\right)^{-1/2}.$$

Understanding Cooling Times

Net power (absorbed minus emitted) by dust in IR:

$$\Lambda_{rad} = n_d(4\pi a^2)\langle Q\rangle\sigma T_d^4 - n_d(\pi a^2)f_* = n_d(4\pi a^2)\langle Q\rangle\sigma(T_d^4 - T_{eq}^4)$$

$$\approx 5.68\times10^{-7}\ \mathrm{W\ m^{-3}\ K^{-1}}\left(\frac{\rho_d}{10^{-8}\ \mathrm{kg\ m^{-3}}}\right)(T_d - T_{eq})\times\begin{cases}\left(\frac{T_g}{100\ \mathrm{K}}\right)^3\left(\frac{a}{1\ \mu\mathrm{m}}\right)^{-1} & \text{for } aT > 600\ \mu\mathrm{m}\cdot\mathrm{K},\\ \left(\frac{T_g}{100\ \mathrm{K}}\right)^4 & \text{for } aT < 600\ \mu\mathrm{m}\cdot\mathrm{K},\end{cases}$$

$$t_d^{rad} = \rho_d c_d/(\Lambda_{rad}/|T_d - T_{eq}|)$$

$$\approx 14\ \mathrm{s}\times\begin{cases}\left(\frac{T_g}{100\ \mathrm{K}}\right)^{-3}\left(\frac{a}{1\ \mu\mathrm{m}}\right) & \text{for } aT > 600\ \mu\mathrm{m}\cdot\mathrm{K},\\ \left(\frac{T_g}{100\ \mathrm{K}}\right)^{-4} & \text{for } aT < 600\ \mu\mathrm{m}\cdot\mathrm{K}.\end{cases}$$

ZVI with Cooling

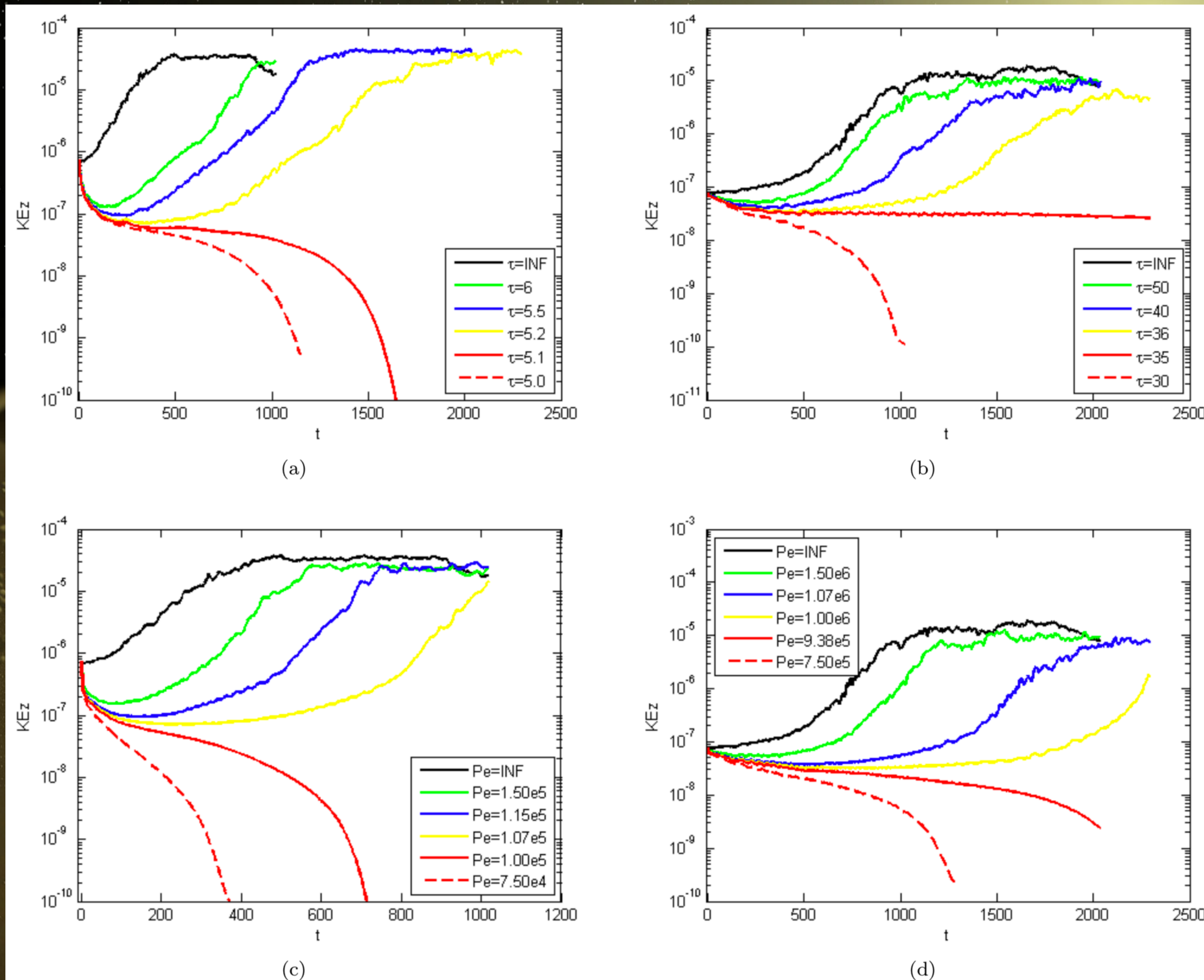

Cooling Times with No Settling

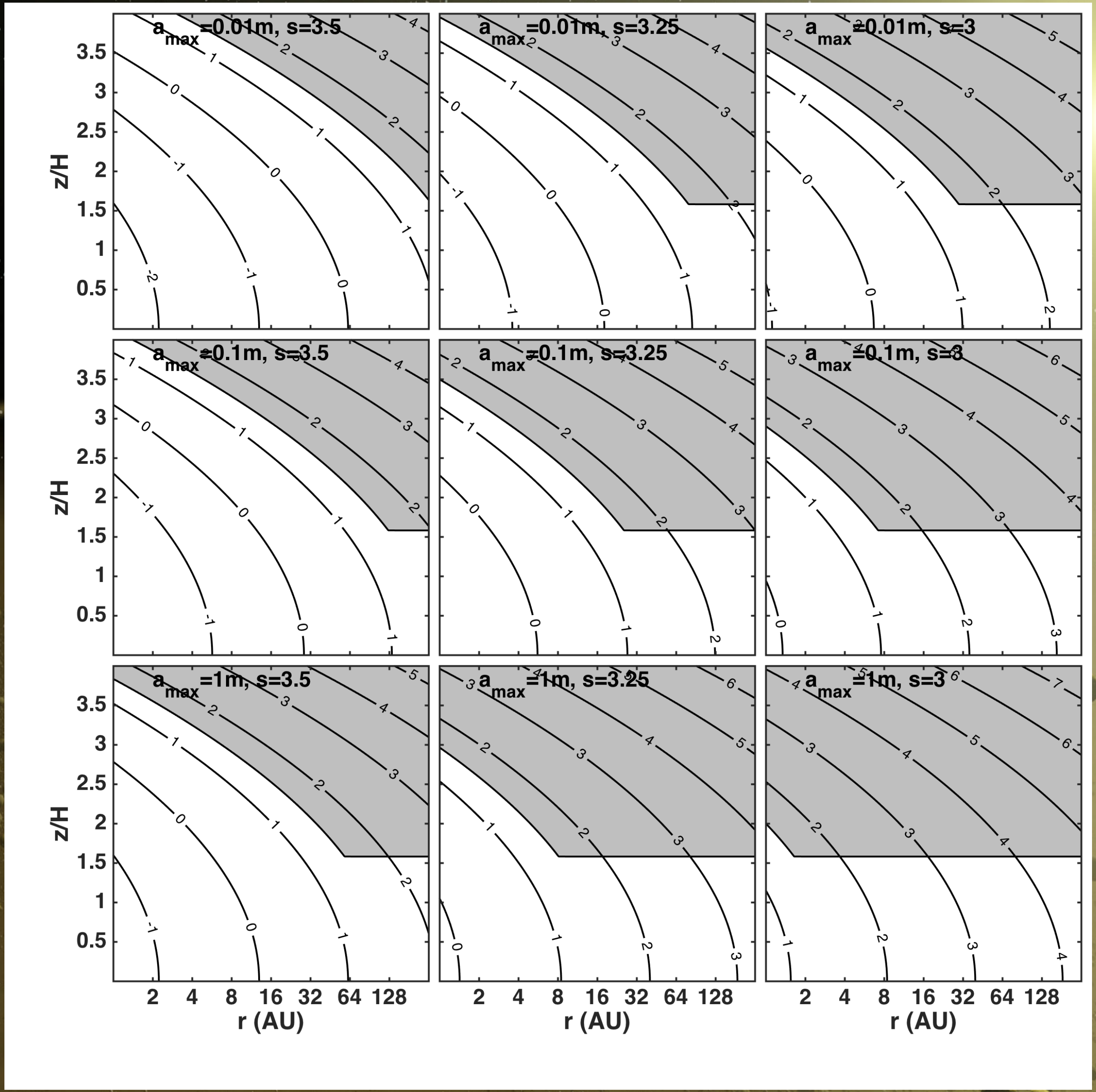

Cooling Times with Settling

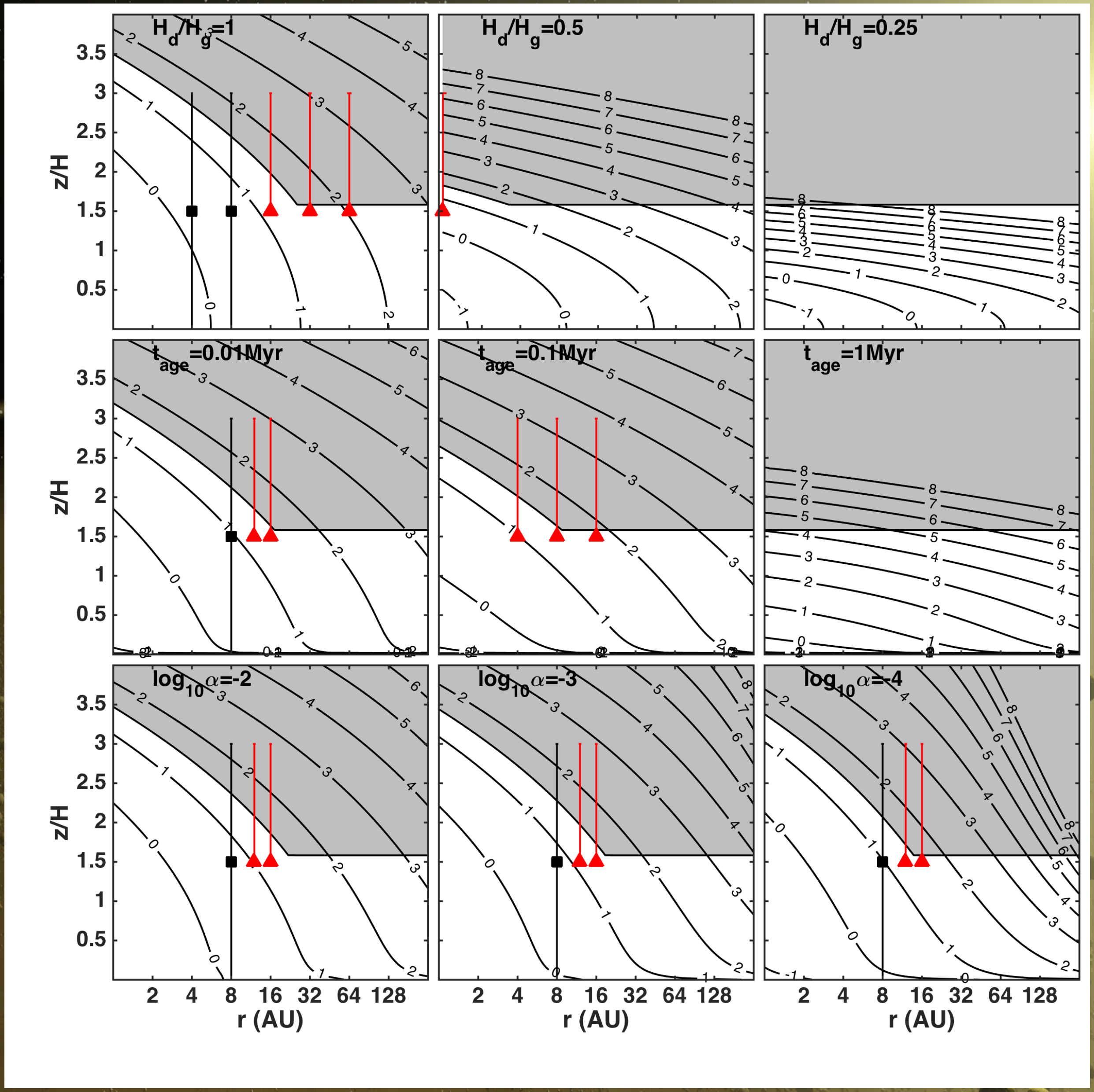

Challenges

- "Local" simulations are good for identifying mechanisms for instability and following evolution into nonlinear and turbulent state.
- But how do we connect "local" simulations with "global" simulations without "smearing" out the resolution necessary for capturing instability processes and turbulent mixing?
- Need more development of subgrid scale models for evolution of dust size distribution that can be implemented in local and global simulations (e.g. Estrada et al. 2015, Tamfal et al. 2018).
- Simulations should include spatio-temporal evolution of cooling times. Evolution of dust size distribution, global spatial evolution of dust via vertical settling, radial migration and turbulent mixing all depend on hydrodynamic and MHD instabilities, yet the prevalence and robustness of these instabilities depend on cooling rates that are set by dust size distribution!

Dimits shift, avalanche-like bursts, and solitary propagating structures in HasegawaWakatani models for plasma edge turbulence

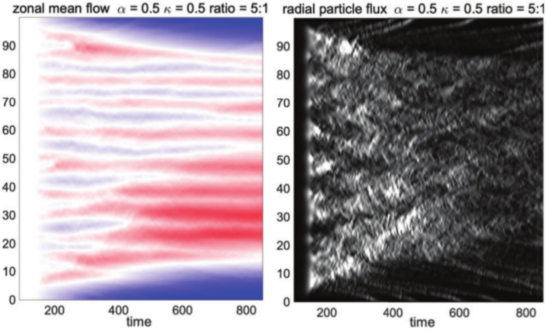

Antoine Cerfon, D. Qi, A. Majda, Courant Institute NYU

KITP Staircase 2021

DRIFT WAVES AND DRIFT INSTABILITY

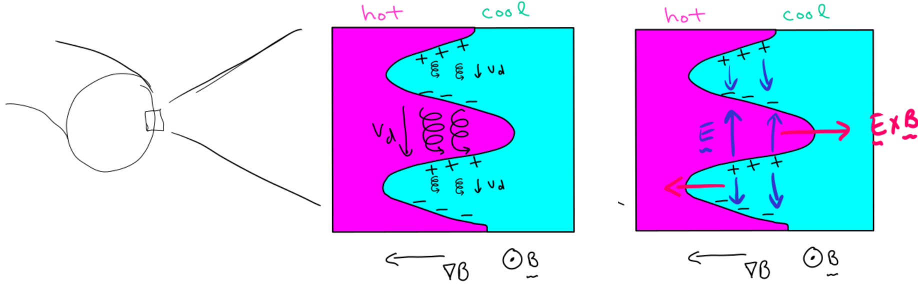

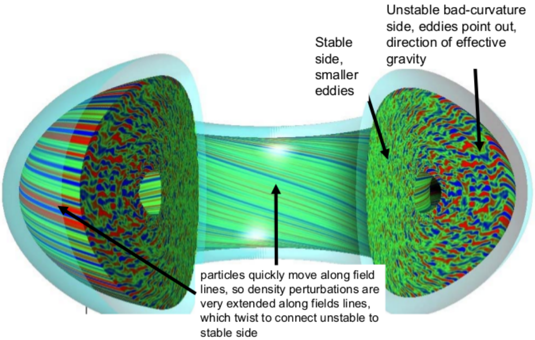

Cartoon picture by G. Hammett (PPPL)

Kinetic simulation by J. Candy and R. Waltz (GA)

Turbulence driven transport

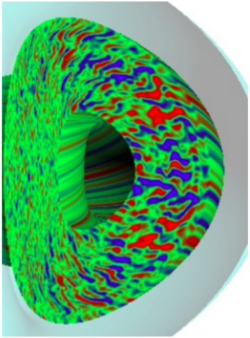

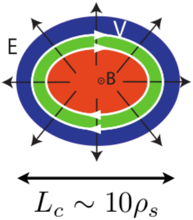

Heuristic picture from Troy Carter (UCLA)

- Random walk by eddy decorrelation
- $D \propto \frac{L_c^2}{\tau_c}$ $\qquad \tau_c \propto \frac{L_c}{v_E} \propto \frac{L_c B}{E} \propto \frac{L_c^2 B}{\phi}$

$$\mathbf{D} \propto \frac{\phi}{B} \propto \frac{T}{B}$$

- D inversely proportional with B. Unfortunate, but expected.
- D proportional with T. Unfortunate, and unexpected: as the plasma gets hotter, confinement degrades
- Transport dominated by turbulent driven transport
- "Low confinement" mode, experimentally verified

A lucky discovery

- "High confinement" regime discovered as input power is increased[1]
- Edge transport barrier, with large gradients[2]
- Strong, cross-field rotation localized in the edge observed [3]

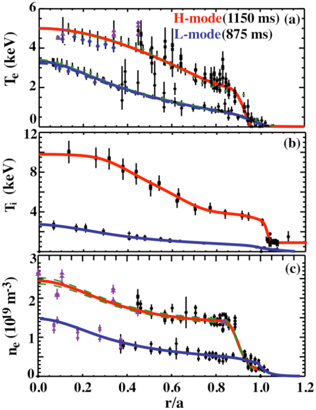

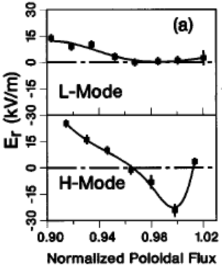

[1] F. Wagner *et al.*, *Physical Review Letters* **49** 1408 (1982)
[2] L. Schmitz *et al.* *Nuclear Fusion* **52** 023003 (2012)
[3] K.H. Burrell, *Physics of Plasmas* **4**, 1499 (1997)

Shear suppression of turbulence

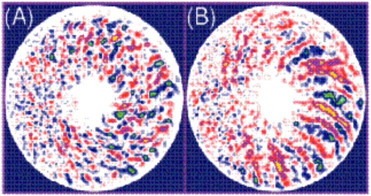

With Flow   Without Flow

Movie 1
Movie 2

- Sheared flow "breaks up" turbulent eddies, smaller eddies mean smaller diffusive step size [4]
- Fundamental role of zonal flows

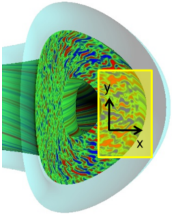

[4] Z. Lin, T. S. Hahm, W. W. Lee, W. M. Tang, R. B. White, *Science* **281**, 1835 (1998)

Nonlinear upshift of critical gradient

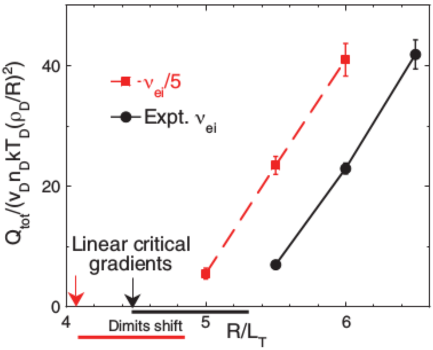

Nonlinear upshift of the critical gradient for the existence of significant transport, a.k.a. "Dimits shift" [5,6].

[5] A Dimits *et al.*, *Physics of Plasmas* **7**, 969 (2000)

[6] D.R. Mikkelsen and W. Dorland, *Physical Review Letters* **101**, 135003 (2008)

Bursty transport & avalanches

- Low-transport regime characterized by nondiffusive, scale-free, and avalanche mediated transport [7]

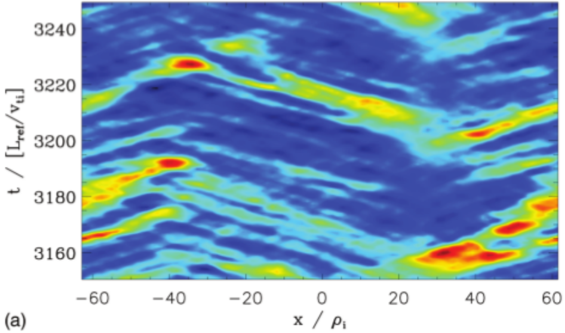

[7] G. Dif-Pradalier *et al.*, *Physical Review E* **82**, 025401(R) (2010)
Tobias Görler *et al.*, *Physics of Plasmas* **18**, 056103 (2011)

Bursty transport & avalanches

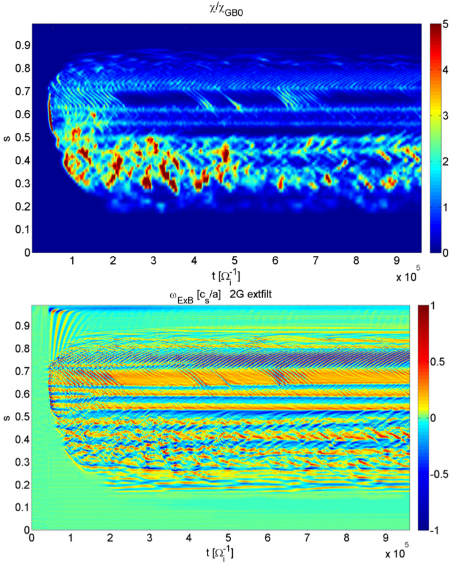

L. Villard *et al.*, *Plasma Physics and Controlled Fusion* **55** (2013) 074017

Bursty transport & avalanches (+ Ferdinons?)

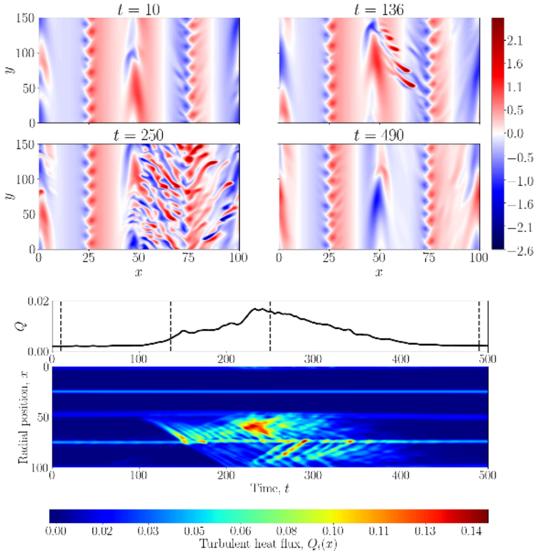

P.G. Ivanov *et al.*, *Journal of Plasma Physics* **86** 855860502 (2020)

INTERMEZZO

Simplest fluid models for zonal flows dynamics

- Two popular models: Hasegawa-Mima and Hasegawa-Wakatani
- Models are NOT accurate for magnetic fusion experiments
- Shearless slab geometry
- Still attractive for their simplicity
  - Better understand drift instability – zonal flow mechanisms
  - Fundamental properties of zonal flows

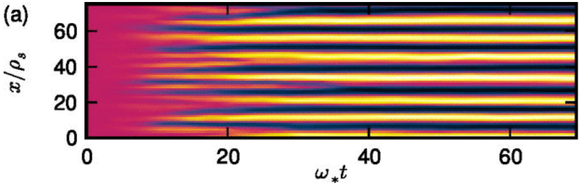

J.B. Parker and J.A. Krommes, *Physics of Plasmas* **20**, 100703 (2013)

Electron dynamics - approximations

- Adiabatic limit= **zero resistivity**
- Small mass $\Rightarrow$ neglect inertia
- Dynamics parallel to the magnetic field
  $eNE_{\parallel} = -\nabla_{\parallel} p_e$
- Assume uniform temperature

$$\nabla_{\parallel}\left(\frac{e\varphi}{T_e}\right) = \frac{\nabla_{\parallel} N}{N} = \nabla_{\parallel} \ln\left(\frac{N}{N_0}\right) \quad \Rightarrow \quad N(x,y,t) = f(x,t)\exp\left(\frac{e\varphi}{T_e}\right)$$

Adiabatic electron response

- Write every quantity as $a = \bar{a} + \tilde{a}$ with $\bar{a} = \frac{1}{L_y}\int_0^{L_y} a dy$

$$N = n_0(x,t)\exp\left(\frac{e\tilde{\varphi}}{T_e}\right) \approx n_0(x,t)(1 + \frac{e\tilde{\varphi}}{T_e})$$

Electron mass conservation

- Mass conservation + Integration by parts:

$$\frac{\partial N}{\partial t} = \frac{\partial \varphi}{\partial y}\frac{\partial N}{\partial x} - \frac{\partial \varphi}{\partial x}\frac{\partial N}{\partial y} \quad \Rightarrow \quad \frac{\partial \overline{N}}{\partial t} = \frac{\partial}{\partial x}\left(\frac{1}{L_y}\int_0^{L_y} N\frac{\partial \tilde{\varphi}}{\partial y}dy\right)$$

- Use $\frac{\partial N}{\partial y} = n_0(x,t)\frac{\partial \tilde{\varphi}}{\partial y}$

$$\frac{\partial \overline{N}}{\partial t} = 0 \qquad \textbf{No net radial electron flux}$$

- Conclude:

  $\Rightarrow \quad N = n_0(x)(1 + \frac{e\tilde{\varphi}}{T_e})$

  $\Rightarrow$ **Solve for normalized density fluctuation** $n = \tilde{n} = \tilde{\varphi}$

Hasegawa-Mima models

$$\frac{\partial q}{\partial t} + J(\varphi, q) - \kappa \frac{\partial \tilde{\varphi}}{\partial y} = 0 \qquad J(\varphi,q) = \partial_x \varphi \partial_y q - \partial_y \varphi \partial_x q \ , \ \kappa = -\frac{\mathrm{d} \ln n_0}{\mathrm{d}x}$$

Original Hasegawa-Mima model[8]: Potential vorticity: $q = \nabla^2 \varphi - \varphi$

- No drift instability – turbulent forcing must be added externally to observe emergence of zonal flows
- Not Galilean invariant for boosts in the y direction
- Unphysical net radial transport of electrons: $\partial \overline{N} / \partial t \neq 0$

Modified Hasegawa-Mima model[9] Potential vorticity: $q = \nabla^2 \varphi - \tilde{\varphi}$

- MHM model has desired Galilean invariance
- No net radial transport of electrons: $\partial \overline{N} / \partial t = 0$
- Stronger zonal flows observed
- Still no drift instability

[8] A. Hasegawa and K. Mima, *Physics of Fluids* **21** 87 (1978)

[9] R.L. Dewar and R.F. Abdullatif in *Frontiers in Turbulence and Coherent Structures* (World Scientific, 2007), pp. 415–430

IMPORTANCE OF PROPER ELECTRON TREATMENT

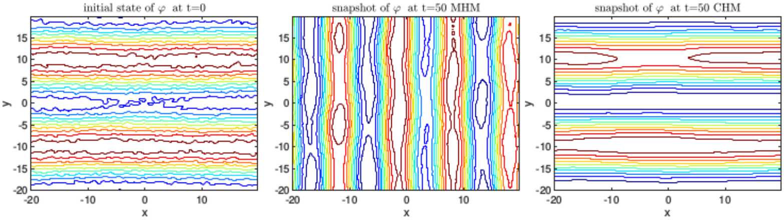

(a) initial drift wave state with wavenumber $s = 2$

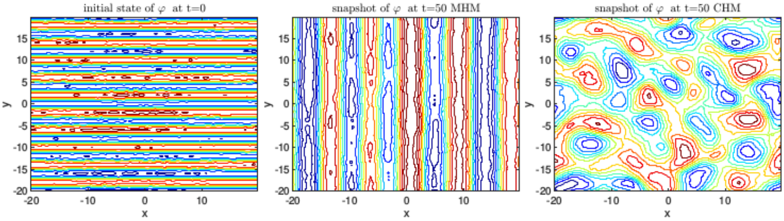

(b) initial drift wave state with wavenumber $s = 10$

D. Qi and A.J. Majda, *Chinese Annals of Mathematics, Series B* **40**, 869(2019)

Hasegawa-Wakatani models

- Equation for potential vorticity $q = \nabla^2\varphi - n$

$$\frac{\partial q}{\partial t} + J(\varphi, q) - \kappa\frac{\partial\tilde{\varphi}}{\partial y} = -D\Delta^4 q$$

$$\frac{\partial n}{\partial t} + J(\varphi, n) + \kappa\frac{\partial\tilde{\varphi}}{\partial y} = \begin{cases} \alpha(\varphi - n) - D\Delta^4 n & \text{Original HW}^{10} \\ \alpha(\tilde{\varphi} - \tilde{n}) - D\Delta^4 n & \text{Modified HW}^{11} \end{cases}$$

  - **Original HW**: NOT Galilean invariant, hard to generate zonal flows
  - **Modified HW**: Galilean invariant, strong zonal flows
- Hasegawa-Mima limit: $\alpha \to \infty$
  - **OHW**: $n \to \varphi$, $q^{OHW} \to \nabla^2\varphi - \varphi = q^{OHM}$

    The OHW model converges to the OHM.
  - **MHW**: $\tilde{n} \to \tilde{\varphi}$, $q^{MHW} \to \nabla^2\varphi - \tilde{\varphi} - \overline{n} \neq q^{MHM}$

    The MHW model may not converge to the MHM model.

[10] A. Hasegawa and M. Wakatani, *Physical Review Letters* **50**, 682 (1983)

[11] R. Numata, R. Ball, and R.L. Dewar, *Physics of Plasmas* **14**, 102312 (2007)

A subtle convergence question

$$\frac{\partial \overline{n}}{\partial t} = \frac{\partial}{\partial x}\left(\frac{1}{L_y}\int_0^{L_y} \tilde{n}\frac{\partial \tilde{\varphi}}{\partial y} dy\right)$$

- If $\alpha = \infty$, $\tilde{n} = \tilde{\varphi} \Rightarrow \frac{\partial \overline{n}}{\partial t} = 0$
- If α is finite, no obvious bound on $\frac{\partial \overline{n}}{\partial t}$

FLUX-BALANCED HASEGAWA-WATANI MODEL [12, 13]

- Fundamental quantities are $q^{\mathrm{b}} = \nabla^2\varphi - \tilde{n}$ and n

$$\frac{\partial q^{\mathrm{b}}}{\partial t} + J\left(\varphi, q^{\mathrm{b}}\right) - \kappa\frac{\partial\tilde{\varphi}}{\partial y} = -D\Delta^4 q^{\mathrm{b}}$$

$$\frac{\partial n}{\partial t} + J\left(\varphi, n\right) + \kappa\frac{\partial\tilde{\varphi}}{\partial y} = \alpha\left(\tilde{\varphi} - \tilde{n}\right) - D\Delta^4 n$$

- The BHW model converges to the MHM model in the appropriate limit, by construction
- MHW model for comparison:

$$\frac{\partial q^{\mathrm{b}}}{\partial t} + J\left(\varphi, q^{\mathrm{b}}\right) + \frac{\partial\left(\overline{\tilde{u}\tilde{n}}\right)}{\partial x} - \left(\kappa - \frac{\partial\overline{n}}{\partial x}\right)\frac{\partial\tilde{\varphi}}{\partial y} = D\Delta q^{\mathrm{b}}$$

- Linear drift instability identical in both models
- Nonlinear dynamics very different

[12] A.J. Majda, D. Qi, and A.J. Cerfon, *Physics of Plasmas* **25**, 102307 (2018)
[13] D. Qi, A.J. Majda, and A.J. Cerfon, *Physics of Plasmas* **26**, 082303 (2019)

Differences between the MHW and BHW models

- Robust zonal flows: In the BHW model, zonal structures observed even in the highly resistive limit[12,13]

BHW model

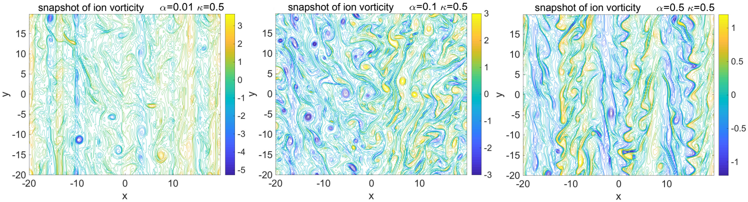

MHW model

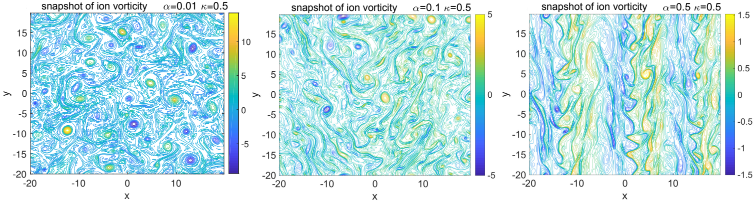

DIFFERENCES BETWEEN THE MHW AND BHW MODELS

Zonal jets are more robust, but also have larger variability[12,13]

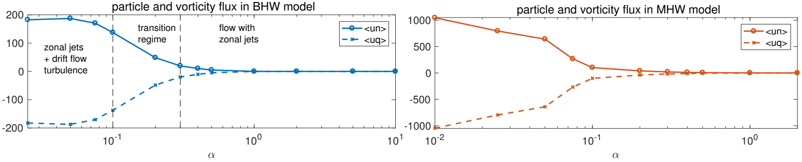

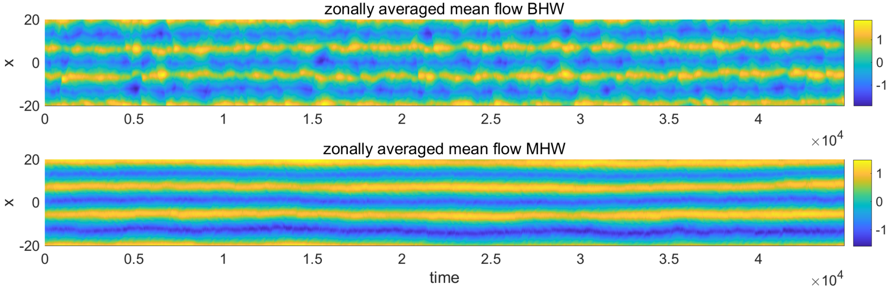

Dimits shift in the BHW model, not in the MHW model[14]

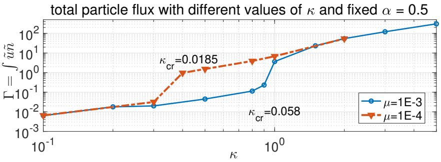

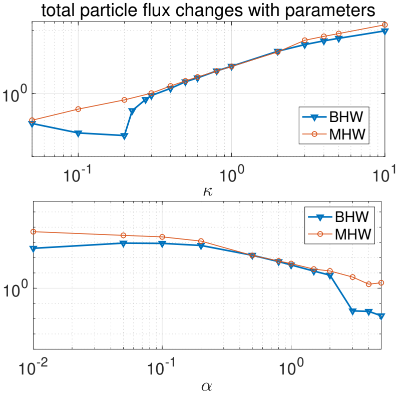

[14] D. Qi, A.J. Majda, and A.J. Cerfon, *Physics of Plasmas* **27**, 102304 (2020)

Radially propagating coherent structures in the BHW model, not in the MHW model[14]

BHW

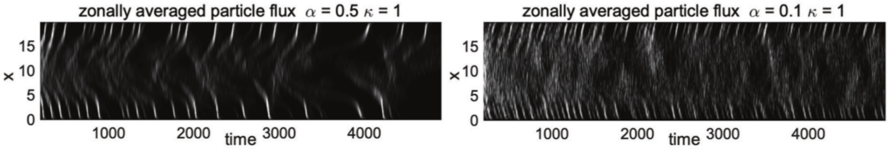

MHW

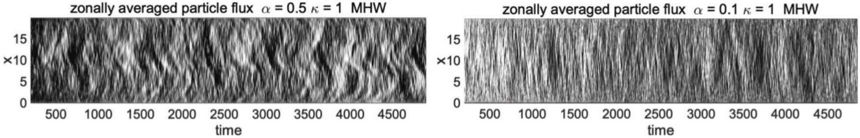

Coherent structures propagate in regions of high shear[14]

BHW Channel Geometry

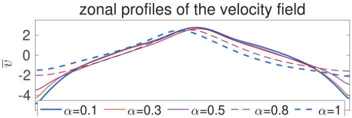

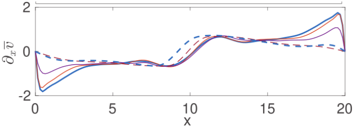

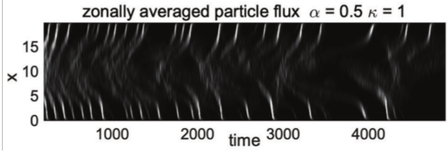

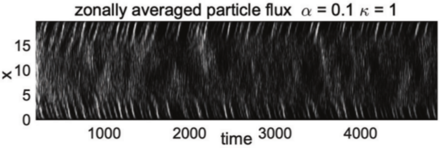

BHW Periodic boundary conditions

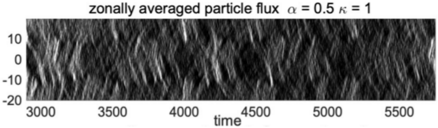

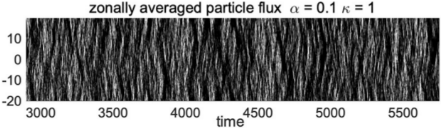

Summary

Transport in tokamaks may be separated into an organized Dimits regime and a strongly turbulent regime.

In the Dimits regime, one oberves periodic bursts in the particle/heat fluxes, with avalanches and coherent solitary structures.

We have presented the only known Hasegawa-Wakatani model with a Dimits shift, avalanches, and coherent solitary structures.

The key to observing these phenomena in the Hasegawa-Wakatani framework is the proper treatment of the parallel electron dynamics.

Strong velocity shear is required for the existence of radially propagating coherent solitary structures.

Capturing negative turbulent viscosity in reduced models of unstable shear flows

Adrian Fraser[1], Paul Terry[2], Ellen Zweibel[2], M.J. Pueschel[3], J.M Schroeder[2], B. Tripathi[2]

[1]UCSC; [2]UW-Madison; [3]DIFFER, Eindhoven University of Technology

March 3, 2021

Shear-flow instabilities drive turbulence, enhance mixing

Below: example of **turbulence driven by unstable shear flow**
$\rightarrow$ enhances mixing beyond diffusion

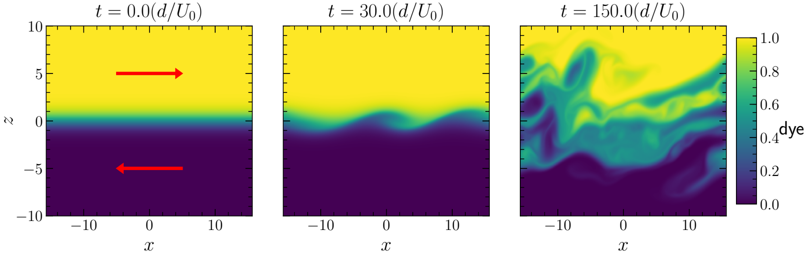

- Turbulent transport: **difficult to predict**
- Natural systems (e.g. stars) often too complex for accurate direct numerical simulations

$\rightarrow$ One **motivation for this work**: need reduced models, tools for predicting behavior when simulations impractical or impossible

MHD KH: weak/moderate $\mathbf{B}_0$ enhances turbulence despite partially stabilizing instability

Palotti et al. 2008: for $\mathbf{B} = 0$ (left), large-scale vortices dominate KH

$\mathbf{B} \neq 0$ (right) increases small-scale fluctuations *despite stabilizing influence*

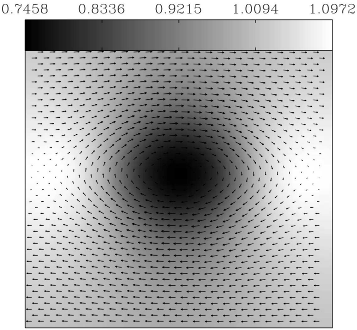

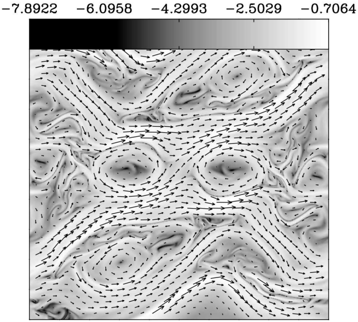

MHD KH: turbulent transport, layer broadening rate increase with field strength

Mak et al. 2017: as $\mathbf{B}_0$ increases (left to right), turbulent momentum transport increases $\rightarrow$ layer broadens faster

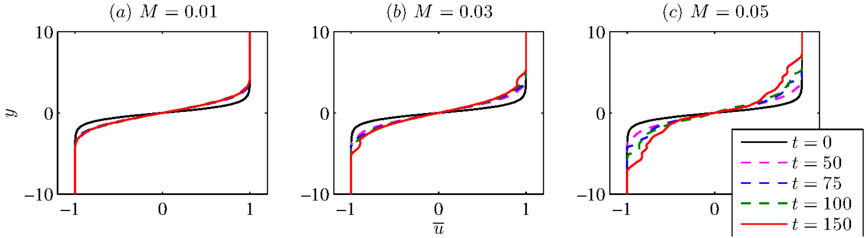

This work: pursue explanation for this counter-intuitive trend $\rightarrow$ might lead to reduced models

Specifically, explore role of stable modes, variation with $\mathbf{B}_0$

Some fluctuations return energy to the driving shear flow

Inviscid shear flows: for every unstable mode there exists a "conjugate" stable mode (tied to PT symmetry, see Qin et al. arXiv:2010.09620)

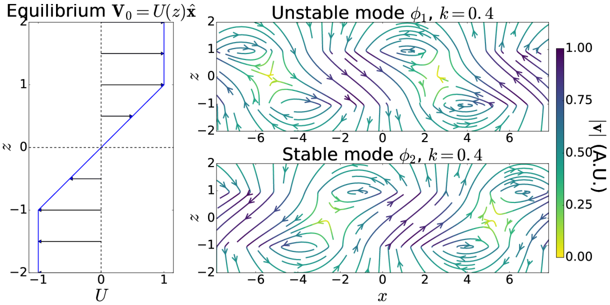

Fraser et al. Phys. Plasmas (2017)

Unstable modes: driven by shear flow

Stable modes: put energy back

Both types present in random perturbations

Unstable modes: $\mathbf{u}(x, z, t) \sim \mathbf{u}_1(z) e^{ik_x x} e^{\gamma t} \rightarrow$ linear growth

Stable modes: $\mathbf{u}(x, z, t) \sim \mathbf{u}_2(z) e^{ik_x x} e^{-\gamma t} \rightarrow$ linear decay

Signatures of stable modes exist in shear flow experiments

Note: energy transfer to/from perturbations $\leftrightarrow$ momentum transport down/up the gradient (Reynolds stress) $\leftrightarrow$ layer broadens/shrinks

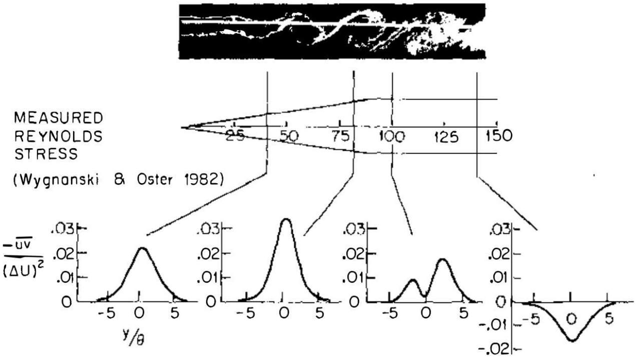

Figure 20 Evolution of Reynolds-stress cross-stream distribution with downstream distance in a forced turbulent mixing layer (from Oster & Wygnanski 1982 and Browand & Ho 1983).

Shear flow experiments: layer broadens first, then sometimes shrinks

(Ho & Huerre Ann. Rev. Fl. Mech. 1984)

2D Kolmogorov flow

Fraser et al. (2018): examine stable modes in 2D Kolmogorov-like flow ($\mathbf{V}_0 \sim \cos(k_x^{\text{eq}} x)\hat{\mathbf{y}}$)

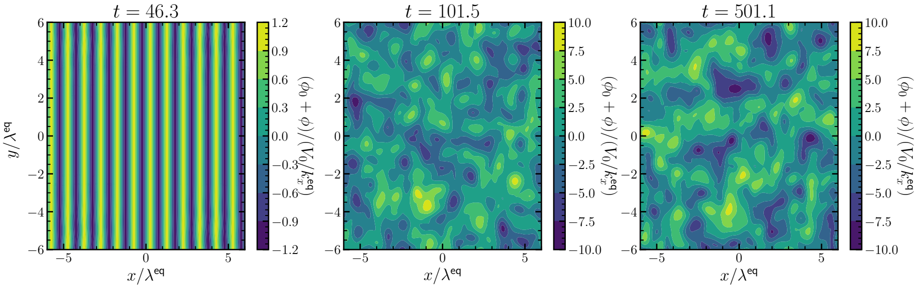

Streamfunction ϕ at three different times

From DNS results, calculate mode amplitudes β_j

At each k_y, t, expand state $\hat{\phi}$ in basis of eigenmodes ϕ_j:

$$\phi_{\mathsf{NL}}(x,y,t) = \sum_{k_y} \hat{\phi}(x,k_y,t)e^{ik_y y} \quad \rightarrow \quad \hat{\phi} = \sum_j \beta_j(t)\phi_j(x)$$

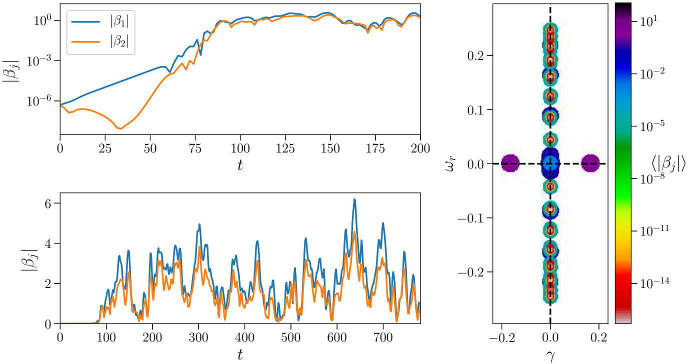

Left: evolution of $\beta_j(t)$ consistent with previous work: β_2 excited by $\beta_1\beta_1$ nonlinear interactions *(think GQL)*

Right: continuum modes ($\gamma = 0$) excited too

$|\beta_2/\beta_1| \approx 1$ in saturation $\Rightarrow$ significant energy transfer *back* to mean flow, β_2 **important in saturating the instability**

ϕ_1, ϕ_2 alone describe some fluctuations well

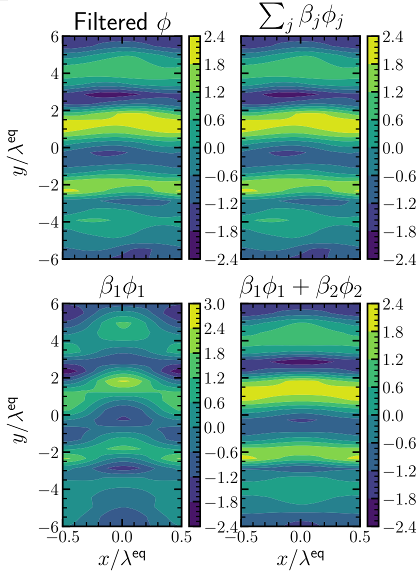

Common assumption in reduced models: $\phi \approx \phi_1$ at large scales
Here: including ϕ_2 yields significant improvements

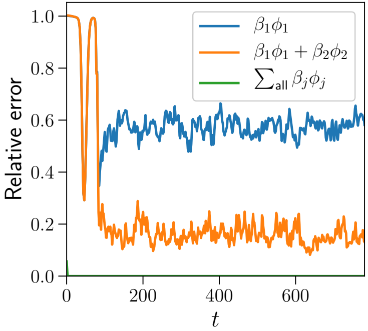

$\phi \approx \beta_1\phi_1 + \beta_2\phi_2$ captures Reynolds stress here $\rightarrow$ what about MHD?

Shear layer with flow-aligned $\mathbf{B}_0$

Simulate a 2D, incompressible, unstratified shear layer in MHD with flow-aligned $\mathbf{B}_0$ in Dedalus (dedalus-project.org):

$$\rho\left(\frac{\partial}{\partial t} + \mathbf{v}\cdot\nabla\right)\mathbf{v} = -\nabla p + \frac{1}{c}\mathbf{J}\times\mathbf{B} + \nu\nabla^2\mathbf{v}$$

$$\frac{\partial}{\partial t}\mathbf{B} - \nabla\times(\mathbf{v}\times\mathbf{B}) = \eta\nabla^2\mathbf{B}$$

$$\nabla\cdot\mathbf{v} = 0$$

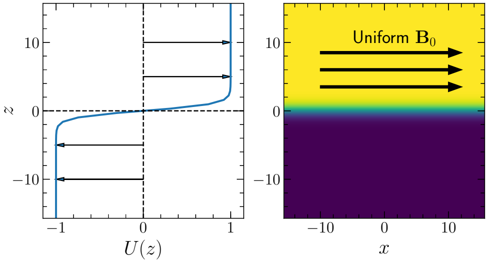

Equilibrium flow:
$\mathbf{V}_0 = U(z)\hat{\mathbf{x}} = U_0\tanh(z/d)\hat{\mathbf{x}}$
Equilibrium field: $\mathbf{B}_0 = B_0\hat{\mathbf{x}}$

Non-dimensionalize in terms of d, U_0, B_0

Model details

Non-dimensionalizing and setting $\mathbf{v} = \hat{\mathbf{y}} \times \nabla\phi$, $\mathbf{B} = \hat{\mathbf{y}} \times \nabla\psi$ yields:

$$\frac{\partial}{\partial t}\nabla^2\phi + \left\{\nabla^2\phi, \phi\right\} = \frac{1}{M_A^2}\left\{\nabla^2\psi, \psi\right\} + \frac{1}{\mathrm{Re}}\nabla^4\phi$$

$$\frac{\partial}{\partial t}\psi = \{\phi, \psi\} + \frac{1}{\mathrm{Rm}}\nabla^2\psi$$

(where $\{f, g\} \equiv \partial_x f \partial_z g - \partial_z g \partial_x f$)

Three free parameters: $M_A \equiv U_0/v_A \propto U_0/B_0$,
$\mathrm{Re} \equiv U_0 d/\nu$,
$\mathrm{Rm} \equiv U_0 d/\eta$

Typically use $\mathrm{Re} = \mathrm{Rm} = 500$

Nonlinear simulations: stronger $\mathbf{B}_0$ enhances layer broadening, eliminates phases of layer shrinking

Assess layer broadening via kinetic energy of the mean flow:
Layer broadening $\leftrightarrow$ reduced $\mathrm{KE}_{k_x=0}$

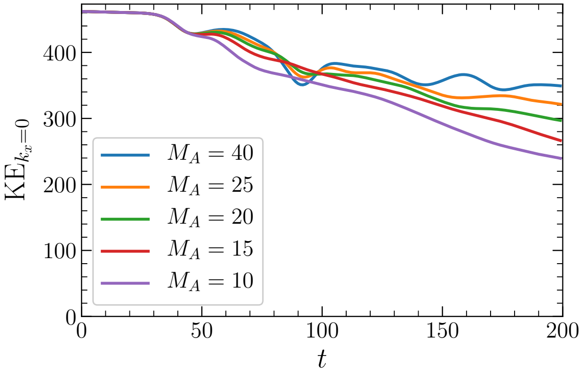

Energy in mean flow decreases faster with stronger magnetic fields

Note local minima in $\mathrm{KE}_{k_x=0}$ $\rightarrow$ negative eddy viscosity $\rightarrow$ stable mode activity

Ideal ($\nu, \eta = 0$) system includes the same stable modes

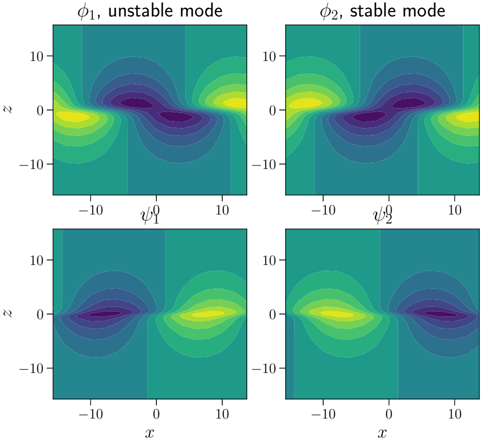

At each unstable k_x, one unstable mode ϕ_1, ψ_1 and conjugate stable mode ϕ_2, ψ_2 with $\gamma_2 = -\gamma_1$

ϕ_1: draws energy from $U(z) \rightarrow$ down-gradient Reynolds/Maxwell stresses
ϕ_2: transfers energy back to $U(z) \rightarrow$ counter-gradient stresses

Calculate eigenmode amplitudes β_j from simulations

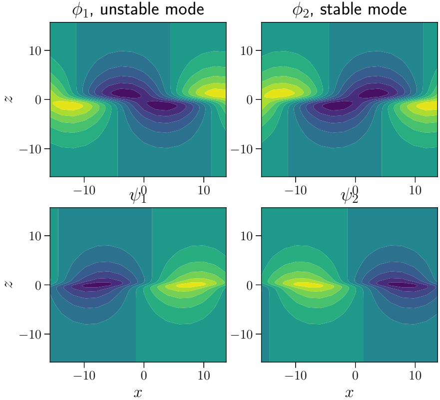

From simulations, calculate **eigenmode amplitudes** β_j

First take FFT: $\phi = \sum_{k_x} \hat{\phi} e^{ik_x x}$

Then expand in ϕ_j basis:

$\hat{\phi} = \sum_j \beta_j \phi_j$

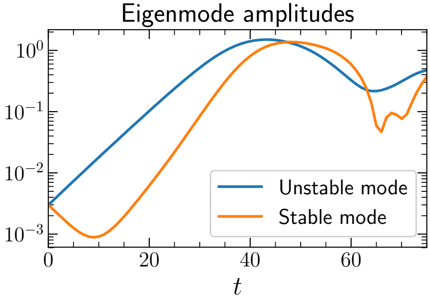

Use to connect Reynolds stress reduction/reversal to stable mode activity
(Also tested with eigenmodes of mean flow $\langle U \rangle_x$ rather than initial U_0)

Unstable, stable mode amplitudes relate directly to Reynolds stress

Consider Reynolds stress $\tau_u \equiv \langle u_x u_z \rangle$ at $z = 0$

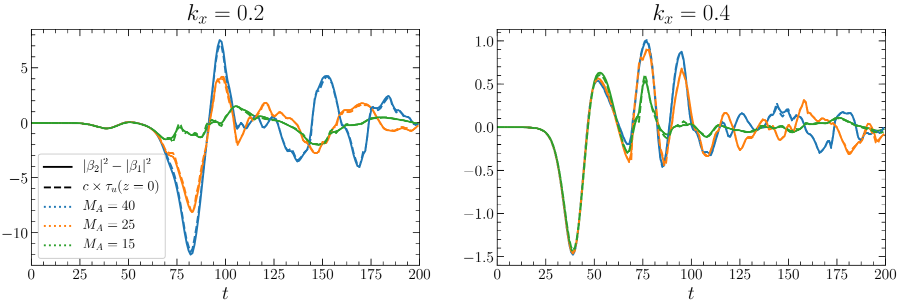

$|\beta_2|^2 - |\beta_1|^2$ yields Reynolds stress at $z = 0$ almost exactly

$\Rightarrow$ Trends in τ_u with B_0 can be understood in terms of B_0 effect on β_2

Enhanced layer broadening due to less counter-gradient Reynolds stress, more down-gradient Maxwell stress

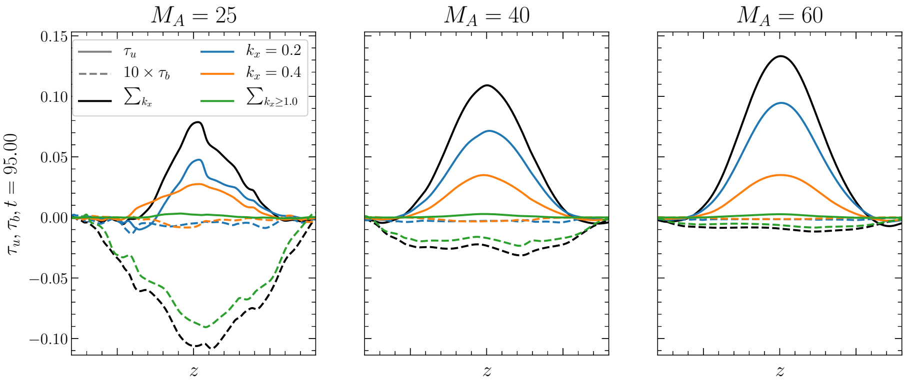

Reynolds stress (solid lines): dominated by large scales (blue, orange), sign implies counter-gradient transport, weaker at stronger fields

Maxwell stress (dashed lines): dominated by small scales (green), always gives down-gradient transport, increases with field strength

Reduced stable mode activity enhances small-scale fluctuations, increases dissipation

With stable modes affecting saturation less at lower M_A, more energy goes to small scales

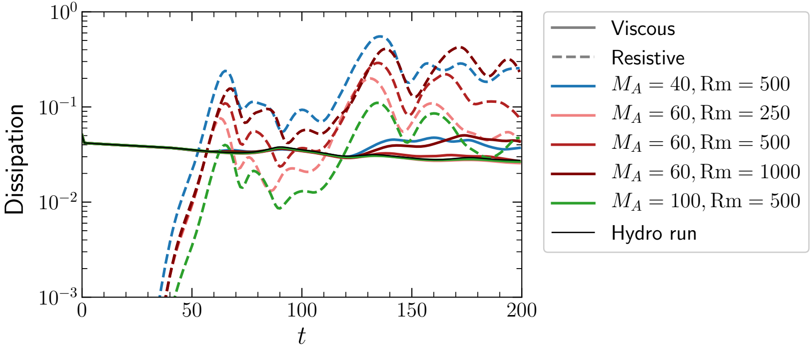

Small-scale fluctuations drive viscous, resistive dissipation

Conclusions

- Stable modes transfer energy back to base flow, produce **counter-gradient momentum transport**
- **Stable modes nonlinearly driven** by unstable modes to significant amplitudes, despite linear stability
- Stable and unstable modes alone describe large-scale fluctuations well

In the MHD case:

- Increased B_0 suppresses stable modes $\rightarrow$ reduces their counter-gradient momentum transport
- Without stable modes, more energy cascades to small scales
- Small-scale fluctuations increase dissipation and down-gradient Maxwell stress

Future directions for this work: MHD problem with reinforced profile, separate model for magnetic fluctuations; **investigate stratified shear flows**

The end

Thank you!

Recently published in Physics of Plasmas, see https://doi.org/10.1063/5.0034575

My email: adfraser@ucsc.edu

Assessing nonlinear coupling for a fixed profile

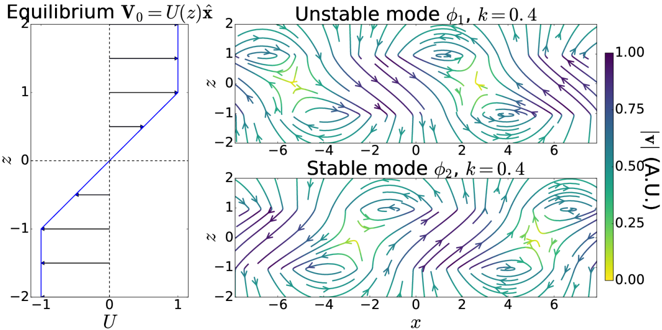

Fraser et al. 2017: analytical calculation of hydro, inviscid, incompressible, 2D, fixed shear layer (ϕ: streamfunction)

At saturation, does more energy go to ϕ_2 or high k_x?

$\rightarrow$ Consider arbitrary linear combination, $\phi(z,t) = \sum_j \beta_j(t)\phi_j(z)$

$\rightarrow$ From vorticity equation, derive eqn for mode amplitudes:

$$\frac{\partial}{\partial t}\nabla^2\phi = \underbrace{\mathcal{L}[\phi]}_{\text{linear terms}} + \underbrace{\mathcal{N}[\phi,\phi]}_{\mathbf{v}\cdot\nabla\mathbf{v}} \rightarrow \frac{\partial}{\partial t}\beta_j = i\omega_j\beta_j + \sum_{m,n} C_{jmn}\beta_m\beta_n$$

Amplitude equations: unstable modes nonlinearly pump stable modes

$$\frac{\partial}{\partial t}\beta_j = i\omega_j\beta_j + \sum_{m,n} C_{jmn}\beta_m\beta_n$$

Nonlinear coupling coefficients C_{jmn}: characterizes energy transfer between ϕ_j, ϕ_m, ϕ_n through $\mathbf{v}\cdot\nabla\mathbf{v}$

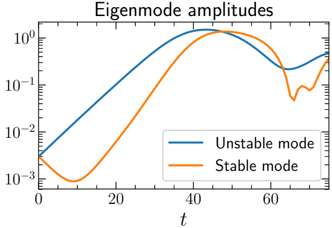

For stable mode $j = 2$:

$$\partial_t\beta_2 = \underbrace{\gamma_2\beta_2}_{\text{inviscid decay}} + \underbrace{C_{211}\beta_1\beta_1}_{\text{NL pumping}} + \ldots$$

Seen in simulations: first $\beta_2 \sim e^{\gamma_2 t}$, then $\beta_2 \sim C_{211}\beta_1\beta_1 \propto e^{2\gamma_1 t}$

Evaluated *threshold parameter* $P_t \sim \frac{\text{stable-unstable couplings}}{\text{unstable-only couplings}}$, found $P_t \gtrsim 0.3$
$\Rightarrow$ **Stable mode coupling significant in saturation**

Track stable mode excitation via DNS

KH in sinusoidal flow ($\mathbf{V}_0 \sim \cos(k_x^{\text{eq}} x)\hat{\mathbf{y}}$): common secondary instability

Tracking stable modes in DNS requires eigenvalue tools, included in gyrokinetic turbulence code GENE (genecode.org)

Fraser et al. (2018): simulate unstable, sinusoidal, **reinforced*** $V_{E\times B}$ shear flow $\rightarrow$ investigate stable modes in post-processing

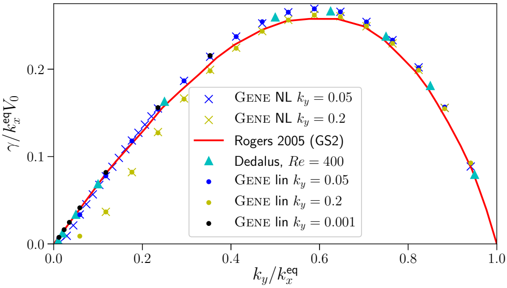

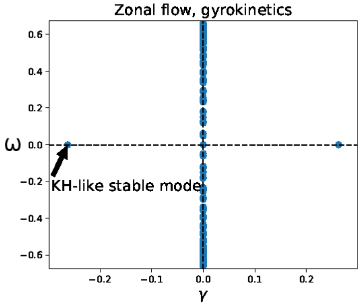

(This is just over-complicated 2D Kolmogorov flow!)

Magnetic field provides stabilizing influence

Calculate eigenmodes for $\mathbf{V}_0 = \tanh(z)\hat{\mathbf{x}}, \mathbf{B}_0 = \hat{\mathbf{x}}$ in Dedalus

System is linearly unstable for $M_A \gtrsim 1\text{-}2$ and $0 < k_x < 1$

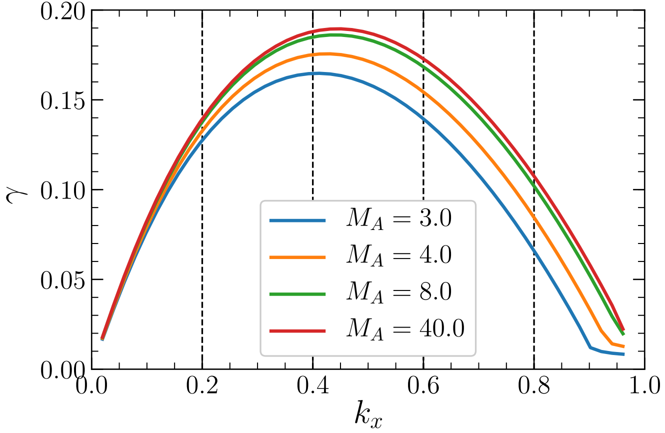

(Dashed lines: wavenumbers in our $L_x = 10\pi$ simulations)